An Iris Recognition System Based on Morphological Operations and Bit Plane Slicing

By

Zahid Hameed

2008-NUST-MS PhD-COM(E)-08

Submitted to the Department of Computer Engineering
in partial fulfillment of the requirements for the Degree of

Masters of Science
In
Computer Engineering

Advisor
Brigadier Dr. Muhammad Younus Javed

Department of Computer Engineering
College of Electrical & Mechanical Engineering
National University of Sciences and Technology (NUST)
2010

Acknowledgements

First of all, I thank to Allah Almighty for his blessings and the strength, he gave to me to accomplish this task. I would like to express my sincere gratitude to my thesis supervisor Brigadier Dr. Muhammad Younus Javed for his skillful guidance and assistance during the course of the project. I appreciate his dedication and interest which made it possible for me to complete the research work well in time. In the course of my master studies, he has provided me with helpful ideas, guidance and comments. He is such a nice, generous and kind hearted person that I really felt comfortable and unconstrained with him during the entire duration of thesis work. Without his invaluable suggestions and continuous guidance I would not have been able to complete my thesis. I owe my research achievements to his experienced supervision. Many thanks to the Guidance and Evaluation Committee (GEC) which includes Dr. Khalid Iqbal (Head of Department), Dr. Almas Anjum and Dr. Assia Khanum for their cooperation, guidance, suggestions and encouragement.

I would also like to thank my friend Dr. Muhammad Salman for supporting and encouraging me generously when it was really required. He was nice enough to spare his precious time from his busy schedule.

A great deal of thanks goes to my parents, in-laws, wife and little daughter, Maryam for their endless support and encouragement even during the most demanding phases of this research. I must acknowledge their sacrifice of time which I owed to them during my research work.

DEDICATION

Dedicated to my family for their support and encouragement

Abstract

An efficient and reliable recognition of an individual is one of the primary objectives of today's high security oriented environment. Biometrics is a technique of measuring an individual's characteristics like face, fingerprints, gait and iris, for its identity. The recognition is done based on some unique characteristic which cannot be transferred or lost. Iris is located in the human eye which consists of highly unique, rich and complex patterns. Iris recognition has proved to be the most accurate methods among the existing biometric technologies which paved its way to the challenging research in the field of digital image processing. The stages of an iris recognition system cover image acquisition, image pre-processing, feature extraction and matching of the iris texture. The performance of the system mainly depends on the removal of noise, correct localization of iris and feature extraction.

In the thesis, pre-processing of the iris region in the image is accomplished by use of the morphological operators and bit plane slicing. The morphological techniques are based on a set theory and are known for their speed as well as accuracy in the image segmentation. The image is probed with a suitable structuring element to perform the operation of dilation and erosion. The iris outer boundary has been detected with the help of a circular summation of the pixel intensities. The experiments have been done on CASIA version 1 iris image dataset. The algorithm has achieved accurate pupil and efficient iris localization when implemented on the dataset.

Bit plane slicing has been used for feature extraction after the normalization of the iris from Cartesian to polar coordinates. Normalization of the iris effective region has been achieved by taking the pupil centre as a reference point. The normalized image is then decomposed into its bit planes. The 8 bits of a 256 level, grayscale image can be decomposed into eight bit planes, i.e. bit plane '1' to bit plane '8'. The higher order bits contribute significantly as compared to the lower order bits. Since the normalized image contains mainly the middle frequencies of the image due to the normalization process of iris so bit plane '5' to bit plane '7' are considered to contain the maximum information for the feature extraction. Bit planes 5 and 6 have been found to provide recognition rate of 98% and 92% respectively as compared to other bit planes for CASIA version 1 dataset.

Table of Contents

CHAPTER 1
INTRODUCTION TO BIOMETRICS

CHAPTER 2
IRIS RECOGNITION SYSTEM – AN OVERVIEW

CHAPTER 3

PROPOSED ALGORITHM

CHAPTER 4

IMPLEMENTATION AND RESULTS

List of Figures

List of Tables

CHAPTER 1

INTRODUCTION TO BIOMETRICS

1.1 What is Biometrics?

The need for the reliable security means and human identification systems has been now considered as one of the primary concerns for any organization in the world due to the prevalent security environment in the world. Traditionally, token and password based systems are used for human identification. The main disadvantage of these systems is that the tokens and passwords can be stolen and guessed. Biometric technology has provided a solution for reliable and efficient security measures because biometric data is unique and cannot be transferred or lost. Biometrics refers to the automated recognition of humans based on some distinctive physiological or behavioral characteristics owned by the individual. The term "biometrics" is a combination of two Greek words that is, bio (life) and metric (to measure). In other words, *bio* means living creature and *metrics* means the ability to measure an object quantitatively [1]. The use of biometrics has been traced back as far as the Egyptians, who measured people to identify them.

The basic principle of working for this technology involves the capturing and processing of an image containing unique features of an individual and comparing it with a processed image captured previously from the database. There are two types of characteristics that is 'behavioral characteristics' are signature or hand writing, typing speed and gait whereas 'physiological characteristics' are the features related to the five senses which includes sight (look of a face, color of eyes or hair, etc), Touch (fingers or palm), Taste (composition of saliva or DNA), Sound (pitch of human voice) and Smell (Odor or sent of a person). All biometric identification systems rely on some forms of random variation among persons based on these characteristics. More complex is the randomness, the more unique features are available for identification; because more dimensions of independent variation produce code having greater uniqueness [2].

In almost each biometric system, an image or sample of the feature which is required to be compared is taken firstly. Then this is converted into a biometric template based on some mathematical transformation. This will allow presenting the most unique

features of the sample for comparison with the stored templates in the system. Thus, the identity is established with the help of some sort of similarity classifier.

A biometric system allows two modes of operation. An enrolment mode for adding templates to a database, and matching mode, where a template is created for an individual and then a match is searched for, in the database of pre-enrolled templates in two ways [1, 8] i.e., identification and verification. In a process of verification (1-to-1 comparison), the biometrics information of an individual, who claims certain identity, is compared with the biometrics on the record that represent the identity that this individual claims. The comparison result determines whether the identity claims shall be accepted or rejected. On the other hand, it is often desirable to be able to discover the origin of certain biometrics information to prove or disprove the association of that information with a certain individual. This process is commonly known as identification (1-to-many comparison). An example of identification is matching of a sketch of an accused by the police officer with the dataset of criminals to find the identity of accused whereas verifying is comparing the individual's face with the photograph available in the passport at the airport by the immigration authorities.

A good biometric is characterized by use of a feature that is: (i) *highly unique* – so that the chance of any two people having the same characteristic will be minimal; (ii) *stable* – so that the feature does not change over time; (iii) be *easily captured* – in order to provide convenience to the user and prevent misrepresentation of the features [3].

1.2 Types of Biometric System

Various types of biometric systems have been developed and most of them have been implemented or are under implementation. Few of these include fingerprint, face, iris, voice, signature and hand geometry. Many other modalities are in various stages of development and assessment. There is not one biometric modality that is best for all implementation. Many factors must be taken into account when implementing a biometric device including location security risks, task (identification or verification), expected number of users, user circumstances, existing data, etc [4]. Some of the major biometric techniques include [5]:-

1.2.1 Face Recognition

Face recognition is one of the oldest and commonly used techniques in the history which is used for the recognition of humans, daily. However, developing face recognition techniques that can allow for the effects of aging, facial expressions, slight variations in imaging and photographing variations in the facial pose is quite challenging. Humans often use faces to recognize individuals and advancements in computing capability over the past few decades, now enable similar recognitions automatically [6, 7]. Early face recognition algorithms used simple geometric models but the face recognition process has now matured into a science of sophisticated mathematical representations and matching processes. Major advancements and initiatives in the past ten to fifteen years have propelled face recognition technology into the spot light.

Figure 1.1. Face image

1.2.2 Finger Print Recognition

Fingerprints are believed to be unique to each person (and each finger). As a result, fingerprinting is one of the most mature biometric technologies used in forensic science worldwide. Fingerprint images are captured, typically, in one of two ways, by scanning an inked impression of a finger or by using a live-scan fingerprint scanner. Recognition through fingerprints is a well-known biometrics technique. Recently due to advancements in computing capabilities it has become automated. Fingerprint identification is popular because of the inherent ease in acquisition, the numerous sources (ten fingers) available for collection, their established use and collections by law enforcement and immigration agencies.

Typical fingerprint recognition methods employ feature-based image matching where minutiae (i.e., ridge ending and ridge bifurcation) are extracted from the registered fingerprint image and the input fingerprint image, and the number of corresponding minutiae pairings between the two images is used to recognize a valid fingerprint image [8].

Figure 1.2. Finger images. a) Using ink. b) Using scanner

1.2.3 Palm Recognition

Palm print recognition inherently implements many of the same matching characteristics that have allowed finger print recognition to be well reputed. Similar to finger, palm biometrics are represented by the information presented in the fiction ridge impression. This information combines ridge flow, ridge characteristics, and ridge structure of the raised portion of the epidermis. The data represented by these fiction ridge impressions allow a determination that corresponding area of fiction ridge impression either originated by the same source or could not have been made by the same source. Palm prints also have uniqueness and permanence [8] like finger prints. However palm recognition has been slower in becoming automated due to some restraints in computing capabilities and live-scan technologies.

1.2.4 Hand/Finger Geometry

People's hands and fingers are unique but not as unique as other traits, like fingerprints or irises. That's why businesses and schools, rather than high-security facilities, typically use hand and finger geometry readers to authenticate users, not to identify them. Disney theme parks, for example, use finger geometry readers to grant ticket holders admittance to different parts of the park. Some businesses use hand geometry readers in place of timecards. Systems that measure hand and finger geometry use a digital camera and light source. To use one, you simply place your hand on a flat

surface, aligning your fingers against several pegs to ensure an accurate reading. Then, a camera takes one or more pictures of your hand and the shadow is casted. It uses this information to determine the length, width, thickness and curvature of your hand or fingers. It translates that information into a numerical template [8, 9].

Hand and finger geometry systems have a few strengths and weaknesses. Since hands and fingers are less distinctive than fingerprints or irises, some people are less likely to feel that the system invades their privacy. However, many people's hands change over time due to injury, changes in weight or arthritis. Some systems update the data to reflect minor changes from day to day.

1.2.5 Voice Recognition

Voice is unique because of the shape of the vocal cavities and the way an individual moves his mouth when he speaks. To enroll in a voiceprint system, either say the exact words or phrases that it requires, or give an extended sample of speech so that the computer can identify no matter which words are said [10, 11]. When people think of voiceprints, they often think of the wave pattern they would see on an oscilloscope. But the data used in a voiceprint is a sound spectrogram, not a wave form. A spectrogram is basically a graph that shows a sound's frequency on the vertical axis and time on the horizontal axis. Different speech sounds create different shapes within the graph. Spectrograms also use colors or shades of grey to represent the acoustical qualities of sound.

However, voiceprints have their own limitations as reproductions of a recorded voice can circumvent a voice authentication system for a remote unattended application [8]. In such cases, additional security may be obtained by varying the spoken sentence.

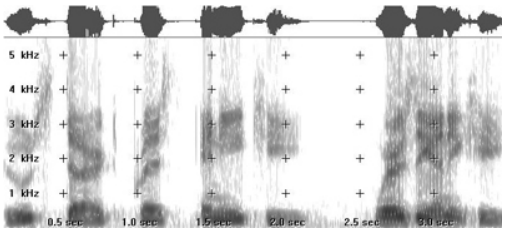

Figure 1.3. Voice spectrograph

1.2.6 Vein Geometry Recognition

As with irises and fingerprints, a person's veins are completely unique. Twins don't have identical veins, and a person's veins differ between their left and right sides. Many veins are not visible through the skin, making them extremely difficult to counterfeit or tamper with. Their shape also changes very little as a person ages [8]. Vein scanners use near-infrared light to reveal the patterns in a person's veins.

To use a vein recognition system, you simply place your finger, wrist, palm or the back of your hand on or near the scanner. A camera takes a digital picture using near-infrared light. The hemoglobin in your blood absorbs the light, so veins appear black in the picture. As with all the other biometric types, the software creates a reference template based on the shape and location of the vein structure.

Figure 1.4. Vein geometry

1.2.7 Handwriting/Signature Recognition

These systems measure the speed and pressure when someone is signing the name (not what the signatures look like) [28]. At first glance, using handwriting to identify people might not seem like a good idea. After all, many people can learn to copy other people's handwriting with a little time and practice. It seems like it would be easy to get a copy of someone's signature or the required password and learn to forge it. But biometric systems don't just look what is the shape of each letter rather they analyze the act of writing. They examine the pressure and the speed and rhythm with which someone writes [8]. They also record the sequence in which an individual forms letter, like whether dots and crosses are added in the writing or not.

Unlike the simple shapes of the letters, these traits are very difficult to forge. Even if someone else got a copy of your signature and traced it, the system probably wouldn't accept the forgery [12, 13]. A handwriting recognition system's sensors can include a touch-sensitive writing surface or a pen that contains sensors that detect angle, pressure and direction. The software translates the handwriting into a graph and recognizes the small changes in a person's handwriting from day to day and over time.

Figure 1.5. Handwriting recognition system

1.2.8 Retinal Recognition

The retinal vasculature is rich in structure and is supposed to be a characteristic of each individual and each eye [8]. It is claimed to be the most secure biometrics since it is not easy to alter or replicate. However, many people are suspicious of retinal scans owing to the fact that retinal vasculature can reveal some medical conditions such as hypertension. This fact presently stands in the way of public acceptance of retinal scan based-biometrics.

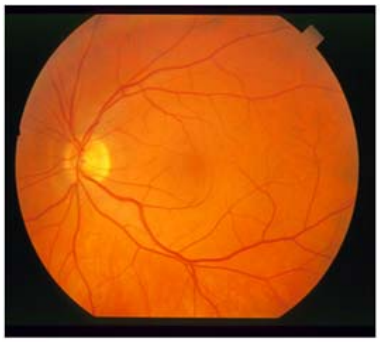

Figure 1.6. Retina image

1.2.9 Key Strokes Recognition

It measures the typing pattern of an individual. This behavioral biometrics offers sufficient discriminatory information to permit for identity authentication [8]. Keystroke dynamic features are based on time durations between the keystrokes. Some variants of identity authentication use features based on inter-key delays as well as dwell times that is how long a person holds down a key.

1.2.10 Gait Recognition

Gait refers to the peculiar way one walks and while it is not claimed to be absolutely unique to each individual, it is sufficiently characteristic to allow for identity authentication [14]. Naturally, gait is a behavioral biometric and may not stay invariant especially over a long period of time due to large fluctuations of body weight and major injuries involving the joints or cerebral disorders. Typically, gait features are derived from analyzing video-sequence footage of a person walking and encompass several characteristic movements of each articulate joint [15].

1.2.11 Facial Thermographs

Thermo gram measures the temperature of the body [8]. The temperature of the face varies with the circulation of blood in the vessels located between the face bones and skin. The skin above the blood vessel is warmer than the adjacent skin on the muscles. The blood vessel pattern is unique for every individual, even in the case of twins. Moreover, the fluctuations in the temperature are also due to the personality and emotional factors.

1.2.12 Ear Recognition

Studies have shown that the shape and structure of the ear are distinctive. In addition, there is supporting evidence which indicates that ears are probably unique to each individual. Ear database is publicly available on the internet [16].

1.2.13 Iris Recognition

Iris recognition is the process of recognizing a person by analyzing the random pattern of the iris [1]. The iris is a muscular structure within the eye that regulates the pupil, controlling the amount of light that enters an eye. It is colored portion of an eye,

although the coloration and the structure of the iris are genetically linked, the details of the pattern are not. Although genetically identical, an individual's irises are unique and structurally distinct which allows them to be used for recognition purpose. In order to obtain a good image of the iris, a recognition system lights up the iris with near infrared light which can be observed by most of the cameras yet it is not detectable nor can it cause injury to human eye [8].

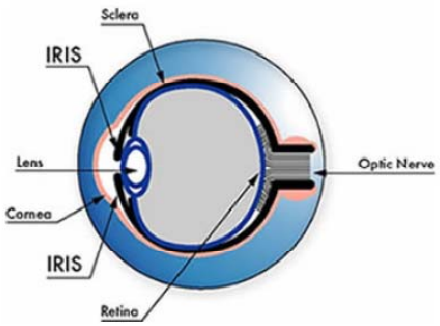

Figure 1.7. Iris image

CHAPTER 2

IRIS RECOGNITION SYSTEM – AN OVERVIEW

2.1 Introduction

Biometric technologies are able to achieve the personal identification and verification based on the physiological and behavioral characteristics of the subject. Currently, there are various biometric technologies, such as fingerprint recognition, face recognition, iris recognition and voice recognition. Some of these technologies are intrusive, like fingerprint recognition, which requires skin contact between the subject and the imaging facility. Some other technologies have relatively low recognition rates, like face recognition and speaker recognition [8].

For the above reasons, iris recognition shows the advantages of non-intrusiveness and higher accuracy [1]. It is non-intrusive, since it only requires the subject to look into the camera for iris image acquisition. It also has a very high identification rate, because of the unique texture patterns and abundant information contained in iris images. Here we give a brief introduction of the iris recognition system and its components as well as a major literature review.

2.2 Anatomy of Iris

The iris is the plainly visible, colored ring that surrounds the pupil. It is a muscular structure that controls the amount of light entering the eye, with intricate details that can be measured. The iris consists of a meshwork of connective tissue, fibers, contraction furrows, crypts, rings, and colorations. All these constitute a distinctive fingerprint that can be seen at a distance from the person. The iris meshwork ensures that a statistical test of independence in two different eyes always passes. This test becomes a rapid visual recognition method. Figure 2.1 shows an human eye characteristics. No two irises are alike. There is no detailed correlation between the iris patterns of even identical twins, or the right and left eye of an individual. The amount of information that can be measured in a single iris is much greater than fingerprints, and the accuracy is greater than DNA [18].

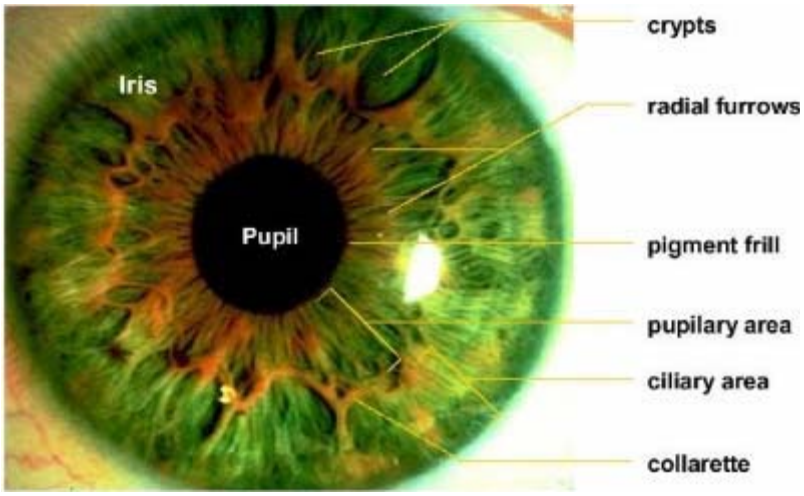

Figure 2.1. Human eye

The iris is a thin circular diaphragm, which lies between the cornea and the lens of a human eye. A front-on view of the iris is shown in Figure 2.1. The iris is perforated close to its centre by a circular aperture known as the pupil. The function of the iris is to control the amount of light entering through the pupil, and this is done by the sphincter and the dilator muscles, which adjust the size of the pupil. The average diameter of the iris is 12 mm, and the pupil size can vary from 10% to 80% of the iris diameter [1].

The iris consists of a number of layers; the lowest is the epithelium layer, which contains dense pigmentation cells. The stromal layer lies above the epithelium layer, and contains blood vessels, pigment cells and the two iris muscles. The density of stromal pigmentation determines the color of the iris. The externally visible surface of the multi-layered iris contains two zones, which often differ in color. An outer ciliary zone and an inner pupillary zone, and these two zones are divided by the collarette – which appears as a zigzag pattern [32].

2.3 Why Iris Recognition?

The iris is the externally-visible, colored ring around the pupil. It is a physical feature of a human being that can be measured and thus used for biometric verification or identification through the process of iris recognition. The human iris is well protected as although it is externally visible, it is an internal part of the eye. It is not genetically determined (which means that genetically identical eyes, e.g. the right and left eye of any

given individual, have unrelated iris patterns) and it is believed to be stable throughout life (barring accidents and surgical operations). Iris patterns are both highly complex and unique [2] (the chance of two irises being identical is estimated at 1 in 10 to the power of 78) making them very well-suited for biometric identification. Iris patterns cannot be modified surgically without unacceptable surgical risk. Moreover, it has been found that the use of contact lenses and glasses does not degrade its performance. The major limitation of the system is, User cooperation, i.e., user has to stand in front of the camera and has to align his eye with the camera.

2.4 How Iris Recognition System Works?

Typically, an iris recognition system consists of five stages:

- Image acquisition.
- Iris preprocessing/localization.
- Normalization.
- Feature extraction.
- Decision and Matching stage.

Figure 2.2 below gives an overview of the complete system. The iris recognition system operates in two modes i.e., Enrollment and Matching mode. In enrollment mode, image is acquired from the subject and processed to localize the iris. Localized iris is normalized to create and store a binary feature vector in the database for future comparison. In matching mode, image is acquired and processed to localize iris effective region which is later normalized to extract the information about features. The extracted features are compared with the templates stored in the database. A score is calculated between two feature vectors of test image and enrolled images in the database one by one. If score is less than a pre-defined threshold than subject is identified otherwise it is considered as a mismatch (here, hamming distance is used to calculate score). The field of iris recognition system has opened a new and active research area in digital image processing and pattern recognition. Some of the existing iris recognition techniques are discussed here briefly.

Figure 2.2. Layout of iris recognition system

2.4.1 Segmentation

In segmentation, it is desired to distinguish the iris texture from the rest of the image. An iris is normally segmented by detecting its inner boundary along the pupil and outer boundary which lies with the sclera. Well-known methods such as the Integro-differential [18], Hough transform [19] and Active contour models [20] have been found successful techniques in detecting the iris boundaries.

2.4.1.1 Daugman's Integro-differential Operator

In order to localize an iris, Daugman proposed the integro-differential operator [2, 18]. The operator assumes that pupil and limbus are circular contours and performs as a circular edge detector. Detecting the upper and lower eyelids are also performed using the integro-differential operator by adjusting the contour search from circular to a designed accurate [9]. The integro-differential is defined as:

— —— (2.1)

The operator pixel-wise searches throughout the raw input image, $I(x, y)$, and obtains the blurred partial derivative of the integral over normalized circular contours in

different radii. The pupil and limbus boundaries are expected to maximize the contour integral derivative, where the intensity values over the circular borders would make a sudden change. $G_\sigma(r)$ is a smoothing function controlled by σ that smoothes the image intensity for a more precise search.

2.4.1.2 Hough Transform

Hough transform is a standard image analysis tool for finding curves that can be defined in a parametrical form such as lines, polynomials and circles. The recognition of a global pattern is achieved using the local patterns. For instance, recognition of a circle can be achieved by considering the strong edges in an image as the local patterns and searching for the maximum value of a circular Hough transform. Wildes et al. [19], Kong and Zhang [21], Tisse et al. [22] and Ma et al. [23] used Hough transform to localize irises. The localization method, similar to Daugman's method, is also based on the first derivative of the image. In the proposed method by Wildes, an edge map of the image is first obtained by applying a threshold equal to the magnitude of the image intensity gradient. From the edge map, votes are casted in Hough space for the parameters of circles passing through each edge point. These parameters are the centre coordinates x_c and y_c, and the radius r, which are able to define any circle according to the equation

$$x_c^2 + y_c^2 - r^2 = 0 \tag{2.2}$$

A maximum point in the Hough space will correspond to the radius and centre coordinates of the circle best defined by the edge points. Wildes et al. and Kong and Zhang also made use of the parabolic Hough transform to detect the eyelids, approximating the upper and lower eyelids with parabolic arcs, which are represented as:

$$(-(x - h_j)\sin\theta_j + (y - k_j)\cos\theta_j)^2 = a_j((x - h_j)\cos\theta_j + (y - k_j)\sin\theta_j) \tag{2.3}$$

In performing the preceding edge detection step, Wildes et al. biased the derivatives in the horizontal direction for detecting the eyelids, and in the vertical direction for detecting the outer circular boundary of the iris. The motivation for this is

that the eyelids are usually horizontally aligned, and also the eyelid edge map will corrupt the circular iris boundary edge map if using all gradient data. Taking only the vertical gradients for locating the iris boundary will reduce influence of the eyelids when performing circular Hough transform, and not all of the edge pixels defining the circle are required for successful localization. Not only does this make circle localization more accurate, it also makes it more efficient, since there are less edge points to cast votes in the Hough space.

There are a number of problems with the Hough transform method. First of all, it requires threshold values to be chosen for edge detection, and this may result in critical edge points being removed, resulting in failure to detect circles/arcs. Secondly, the Hough transform is computationally intensive due to its 'brute-force' approach, and thus may not be suitable for real time applications.

2.4.1.3 Discrete Circular Active Contours

Ritter proposed an active contour model to localize iris in an image [20]. The model detects pupil and limbus by activating and controlling the active contour using two defined forces: internal and external forces. The internal forces are designed to expand the contour and keep it circular. The force model assumes that pupil and limbus are globally circular, rather than locally, to minimize the undesired deformations due to specular reflections and dark patches near the pupil boundary. The contour detection process of the model is based on the equilibrium of the defined internal forces with the external forces. The external forces are obtained from the grey level intensity values of the image and are designed to push the vertices inward. Each vertex is moved between time t and t + 1 by

$$v_i(t+1) = v_i(t) + F_i(t) + G_i(t) \tag{2.4}$$

where F_i is the internal force, G_i is the external force and v_i is the position of vertex i.

For localization of the pupil region, the internal forces are calibrated so that the contour forms a globally expanding discrete circle. The external forces are usually found

using the edge information. In order to improve accuracy Ritter et al. used the variance image rather than the edge image.

A point interior to the pupil is located from a variance image and then a discrete circular active contour (DCAC) is created with this point at its centre. The DCAC is then moved under the influence of internal and external forces until it reaches equilibrium and the pupil is localized.

2.4.1.4 Other Segmentation Methods

Other researchers used methods similar to the segmentation methods described above in the form of modified version. For instance, the iris localization proposed by Tisse et al. is a combination of the integro-differential and the Hough transform. The Hough transform is used for a quick guess of the pupil center and then the integro-differential is used to accurately locate pupil and limbus using a smaller search space [22].

Lim et al. [25] localized pupil and limbus by providing an edge map of the intensity values of the image. The center of pupil is then chosen using a bisection method that passes perpendicular lines from every two points on the edge map. The center point is then obtained by voting the point that has the largest number of line crossovers. The pupil and limbus boundaries are then selected by increasing the radius of a virtual circle with the selected center point and choosing the two radii that have the selected center point and choosing the two radii that have the maximum number of edge-crosses by the virtual circle as the pupil and limbus radii.

2.4.2 Normalization

Normalization refers to preparing a segmented iris image for the feature extraction process. The dimensional variations in the iris occur due to the varying distance between the camera and eye during the process of capturing an eye image. Moreover, illumination has a direct impact on pupil size and causes non-linear variations of the iris patterns. A proper normalization technique is expected to transform the iris image to compensate these variations.

2.4.2.1 Daugman's Rubber Sheet Model

Daugman's normalization method transforms a localized iris texture from Cartesian to polar coordinates [18]. The proposed method is capable of compensating the unwanted variations due to distance of eye from camera (scale) and its position with respect to the camera (translation). The Cartesian to polar transform is defined as:

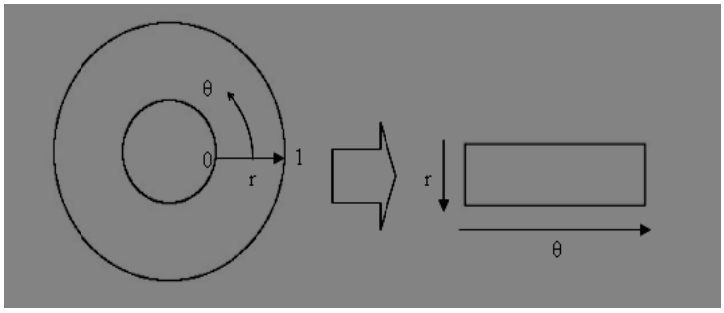

Figure 2.3. Daugman's rubber sheet model

(2.5)

(2.6)

where

The homogenous rubber sheet model devised by Daugman [18] remaps each point within the iris region to a pair of polar coordinates (r, θ) where r is between the interval [0, 1] and θ is angle between [0, 2π]. The process is inherently dimensionless in the angular direction. In the radial direction, the texture is assumed to change linearly which is known as the rubber sheet model.

2.4.2.2 Image Registration

The Wildes et al. [19] system employs an image registration technique, which geometrically warps a newly acquired image, into alignment with a selected database image. When choosing a mapping function to transform the original coordinates, the image intensity values of the new image are made to be close to those of corresponding points in the reference image. The mapping function must be chosen so as to minimize

$$\int_x \int_y (I_d(x,y) - I_a(x-u, y-v))^2 dx\, dy \tag{2.7}$$

while being constrained to capture a similarity transformation of image coordinates *(x, y)* to *(x', y')* that is

$$\begin{pmatrix} x' \\ y' \end{pmatrix} = \begin{pmatrix} x \\ y \end{pmatrix} - sR(\emptyset) \begin{pmatrix} x \\ y \end{pmatrix} \tag{2.8}$$

with *s* is a scaling factor and *R(φ)* is a matrix representing rotation by φ. In implementation, given a pair of iris images I_a and I_d, the warping parameters s and φ are recovered via an iterative minimization procedure.

2.4.2.3 Virtual Circles

In the Boles [24] system, iris images are first scaled to have constant diameter so that when comparing two images, one is considered as the reference image. This works differently to the other techniques, since normalization is not performed until attempting to match two iris regions rather than performing normalization and saving the result for later comparisons. Once the two irises have the same dimensions, features are extracted from the iris region by storing the intensity values along virtual concentric circles with origin at the centre of the pupil. A normalization resolution is selected so that the number of data points extracted from each iris is the same. This is essentially the same as Daugman's rubber sheet model; however, scaling is at match time and is relative to the comparing iris region rather than scaling to some constant dimensions. Also, it is not mentioned by Boles, how rotational invariance is obtained?

2.4.2.4 Li Ma's Method

Ma [23] used a combination of methods of iris normalization that were proposed by Daugman [18] and Bole [24]. In this method, the normalization process is carried out by using center of the pupil as a reference point.

2.4.2.5 Other Methods

Other methods of iris normalization are almost the same as proposed by Daugman. The normalization method makes the iris invariant to scale, translation and pupil dilation changes. The rectangular image after normalization is not rotation invariant. In general, circular shift in different directions is used for achieving rotation invariance during matching process.

2.4.3 Feature Extraction

Once the iris has been localized successfully with its parameters then only the most discriminating features are extracted for recognition purpose. These features are required to be compared with the stored template using some similarity measure to find the score. The score should be different for the intra class and inter class comparison of the subjects.

2.4.3.1 Wavelets

Wavelets can be used to decompose the data in the iris region into components that appear at different resolutions. Wavelets have the advantage over traditional Fourier transform in that the frequency data is localized, allowing features which occur at the same position and resolution to be matched up. A number of wavelet filters, also called a bank of wavelets, is applied to the 2D iris region, one for each resolution with each wavelet a scaled version of some basis function. The output of applying the wavelets is then encoded in order to provide a compact and discriminating representation of the iris pattern.

2.4.3.2 Gabor Filters

A well known iris texture extraction method is proposed by John Daugman [18], who makes use of a decomposition derived from application of a two dimensional version of

Gabor filters to the image data to extract its phase information. Gabor elementary functions are Gaussians modulated by oriented complex sinusoidal functions. Hamming Distance is then used for classification.

Gabor filters are able to provide optimum conjoint representation of a signal in space and spatial frequency. A Gabor filter is constructed by modulating a sine/cosine wave with a Gaussian. This is able to provide the optimum conjoint localization in both space and frequency, since a sine wave is perfectly localized in frequency, but not localized in space. Modulation of the sine with a Gaussian provides localization in space, though with loss of localization in frequency. Decomposition of a signal is accomplished using a quadrature pair of Gabor filters, with a real part specified by a cosine modulated by a Gaussian, and an imaginary part specified by a sine modulated by a Gaussian. The real and imaginary filters are also known as the even symmetric and odd symmetric components respectively.

Daugman demodulates the output of the Gabor filters in order to compress the data. This is done by quantizing the phase information into four levels, for each possible quadrant in the complex plane. Taking only the phase will allow encoding of discriminating information in the iris, while discarding redundant information such as illumination, which is represented by the amplitude component.

These four levels are represented using two bits of data, so each pixel in the normalized iris pattern corresponds to two bits of data in the iris template. A total of 2,048 bits are calculated for the template, and an equal number of masking bits are generated in order to mask out corrupted regions within the iris. This creates a compact 256-byte template, which allows for efficient storage and comparison of irises. The Daugman's system makes use of polar coordinates for normalization.

2.4.3.3 Log-Gabor Filters

A disadvantage of the Gabor filter is that the even symmetric filter will have a DC component whenever the bandwidth is larger than one octave [1]. However, zero DC component can be obtained for any bandwidth by using a Gabor filter which is Gaussian on a logarithmic scale, this is known as the Log-Gabor filter. The frequency response of a Log-Gabor filter is given as:

$$G(f) = \exp\left[\frac{-(\log(\frac{f}{f_0}))^2}{2(\log(\frac{\sigma}{f_0}))^2}\right] \quad (2.9)$$

where f_0 represents the centre frequency, and σ gives the bandwidth of the filter. Details of the Log-Gabor filter are examined by Field.

2.4.3.4 Zero-crossings of the 1D Wavelet

Boles and Boashash [24] made use of 1D wavelet for encoding iris pattern data. The mother wavelet is defined as the second derivative of a smoothing function θ(x).

$$\psi(x) = d^2\theta(x) / dx^2 \quad (2.10)$$

The zero crossings of dyadic scales of these filters are then used to encode features. The wavelet transform of a signal *f(x)* at scale *s* and position *x* is given by

$$W_s f(x) = f * \left[s^2 \frac{d^2\theta(x)}{dx^2}\right](x) = s^2 \frac{d^2}{dx^2}(f * \theta_s)(x) \quad (2.11)$$

where $\theta_s = \left(\frac{1}{s}\right)\theta(\frac{x}{s})$

$W_s f(x)$ is proportional to the second derivative of *f(x)* smoothed by $\theta_s(x)$, and the zero crossings of the transform correspond to points of inflection in $f*\theta_s(x)$. The motivation for this technique is that zero-crossings correspond to significant features with the iris region.

2.4.3.5 Haar Wavelet

Lim et al. [25] also used the wavelet transform to extract features from the iris region. Both the Gabor transform and the Haar wavelet are considered as the mother wavelet. From multi-dimensionally filtering, a feature vector with 87 dimensions is computed. Since each dimension has a real value ranging from -1.0 to +1.0, the feature

vector is sign quantized so that any positive value is represented by 1 and negative value as 0. This results in a compact biometric template consisting of only 87 bits. Lim et al. compared the use of Gabor transform and Haar wavelet transform, and showed that the recognition rate of Haar wavelet transform is slightly better than Gabor transform by 0.9%.

2.4.3.6 Laplacian of Gaussian Filters

In order to encode features, the Wildes et al. system decomposes the iris region by application of Laplacian of Gaussian filters to the iris region image. The filters are given as:

$$\nabla G = -\frac{1}{\pi\sigma^4}\left[1-\frac{\rho^2}{2\sigma^2}\right]e^{-\frac{\rho^2}{2\sigma^2}} \tag{2.12}$$

where σ is the standard deviation of the Gaussian and ρ is the radial distance of a point from the centre of the filter.

The filtered image is represented as a Laplacian pyramid which is able to compress the data so that only significant data remains. A Laplacian pyramid is constructed with four different resolution levels in order to generate a compact iris template.

2.4.4 Matching Algorithms

2.4.4.1 Hamming Distance

The Hamming distance gives a measure of how many bits are the same between two bit patterns. Using the Hamming distance of two bit patterns, a decision can be made as to whether the two patterns were generated from different irises or from the same one. In comparing the bit patterns *X* and *Y*, the Hamming distance, *HD*, is defined as the sum of disagreeing bits (sum of the exclusive-OR between *X* and *Y*) over *N*, the total number of bits in the bit pattern.

$$HD = \frac{1}{N} \times \sum_{i=1}^{N} X_i \,(XOR) Y_i \tag{2.13}$$

Since an individual iris region contains features with high degrees of freedom, each iris region will produce a bit-pattern which is independent to that produced by another iris, on the other hand, two iris codes produced from the same iris will be highly correlated.

If two bits patterns are completely independent, such as iris templates generated from different irises, the Hamming distance between the two patterns should equal to 0.5. This occurs because independence implies the two bit patterns will be totally random, so there is 0.5 chance of setting any bit to 1, and vice versa. Therefore, half of the bits will agree and half will disagree between the two patterns. If two patterns are derived from the same iris, the Hamming distance between them will be close to 0.0, since they are highly correlated and the bits should agree between the two iris codes.

The Hamming distance is the matching metric employed by Daugman [2, 18], and calculation of the Hamming distance is taken only with bits that are generated from the actual iris region.

2.4.4.2 Weighted Euclidean Distance

The weighted Euclidean distance (WED) can be used to compare two templates, especially if the template is composed of integer values. The weighting Euclidean distance gives a measure of how similar a collection of values are between two templates. This metric has been employed by Zhu et al. [26] and is specified as:

$$WED\ (k) = \sum_{i=1}^{N} \frac{(f - f_i^{(k)})^2}{(\delta_i^{(k)})^2} \tag{2.14}$$

where f_i is the i[th] feature of the unknown iris and $\boldsymbol{f_i^{(k)}}$ is the i[th] feature of iris template, k and $\boldsymbol{\delta_i^{(k)}}$ is the standard deviation of the i[th] feature in iris template *k*. The unknown iris template is found to match iris template *k*, when WED is a minimum at *k*.

2.4.4.3 Normalized Correlation

Wildes et al. made use of normalized correlation between the acquired and database representation for goodness of match. This is represented as:

$$\frac{\sum_{i=1}^{n}\sum_{j=1}^{m}(p_1[i,j]-\mu_1)(p_2[i,j]-\mu_2)}{nm\sigma_1\sigma_2} \tag{2.15}$$

where p_1 and p_2 are two images of size n x m, μ_1 and σ_1 are the mean and standard deviation of p_1, and μ_2 and σ_2 are the mean and standard deviation of p_2.

Normalized correlation is advantageous over standard correlation, since it is able to account for local variations in image intensity that corrupt the standard correlation calculation.

CHAPTER 3
PROPOSED ALGORITHM

Iris recognition requires that the localization of the pupil and iris be carried out accurately since the accuracy of whole system is dependent on this first stage. The implementation of pupil localization has been done by using the morphological operators and bit plane. The iris outer boundary has been accomplished by the use of Gaussian blur and then finding the maximum difference after circular summation of the pixel intensities. The normalization process has been done using Daugman's rubber sheet model. The feature extraction has been done using the bit plane slicing of the normalized image and comparison has been made by hamming distance. The proposed algorithm has been tested on CASIA version 1 image dataset.

3.1 Morphological Operators

Morphology is a broad set of image processing operations that process images based on shapes [27]. Morphological operations apply a structuring element to an input image, creating an output image of the same size. In a morphological operation, the value of each pixel in the output image is based on a comparison of the corresponding pixel in the input image with its neighbors. By choosing the size and shape of the neighborhood, you can construct a morphological operation that is sensitive to specific shapes in the input image.

3.1.1 Erosion

Erosion is one of the two basic operators in the area of mathematical morphology, the other being dilation. It is typically applied to binary images, but there are versions that work on grayscale images. The basic effect of the operator on a binary image is to erode away the boundaries of regions of foreground pixels (*i.e.* white pixels, typically). Thus areas of foreground pixels shrink in size, and holes within those areas become larger [27]. The erosion operator takes two pieces of data as inputs. The first is the image which is to be eroded. The second is a (usually small) set of coordinate points known as a

structuring element (also known as a kernel). It is this structuring element that determines the precise effect of the erosion on the input image.

As an example of binary erosion, suppose that the structuring element is a 3×3 square, with the origin at its center as shown in Figure 3.1. Foreground pixels are represented by 1's and background pixels by 0's.

1	1	1
1	1	1
1	1	1

Figure 3.1. A 3×3 square structuring element.

To compute the erosion of a binary input image by this structuring element, we consider each of the foreground pixels in the input image in turn. For each foreground pixel (which we will call the input pixel) we superimpose the structuring element on top of the input image so that the origin of the structuring element coincides with the input pixel coordinates. If for *every* pixel in the structuring element, the corresponding pixel in the image underneath is a foreground pixel, then the input pixel is left as it is. If any of the corresponding pixels in the image are background, however, the input pixel is also set to background value as shown in the Figure 3.2 below.

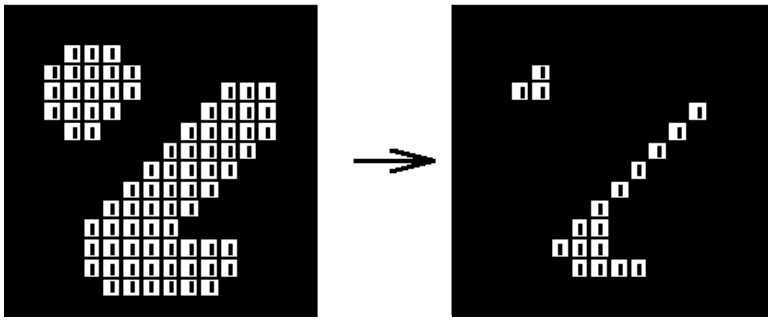

Figure 3.2. Erosion by 3 x 3 square structuring element.

The structuring element may have to be supplied as a small binary image, or in a special matrix format, or it may simply be hardwired into the implementation, and structuring elements do not require specifying at all. In this latter case, a 3×3 square structuring element is normally assumed which gives the shrinking effect. The effect of erosion using this structuring element on a binary image is shown in Figure 3.3.

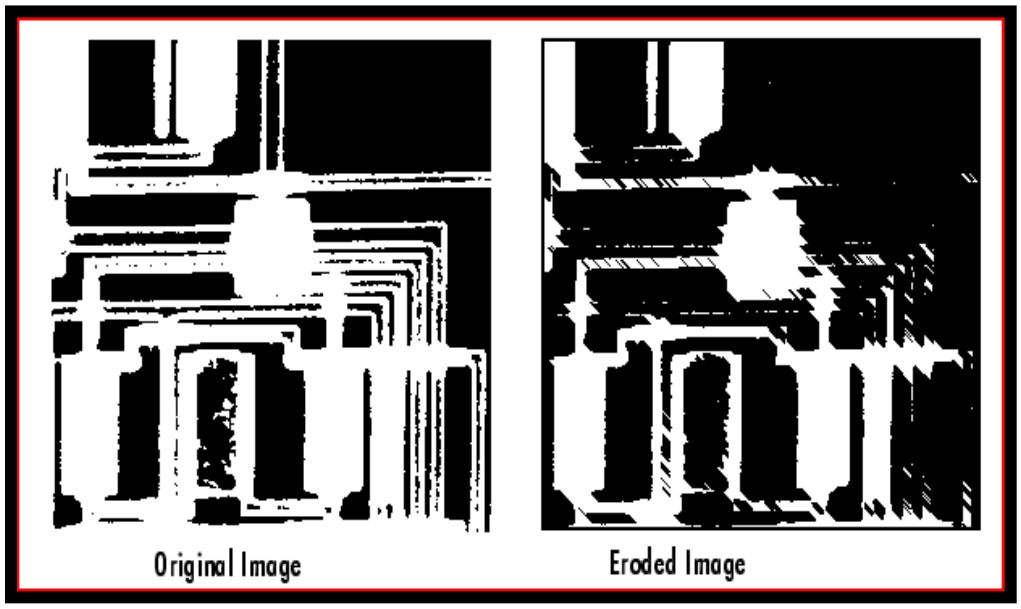

Figure 3.3. Effect of erosion using a 3×3 square structuring element.

The 3×3 square is probably the most common structuring element used in erosion operations but others can also be used. A larger structuring element produces a more extreme erosion effect although usually very similar effects can be achieved by repeated erosions using a smaller similarly shaped structuring element. With larger structuring elements, it is quite common to use an approximately disk shaped structuring element, as opposed to a square one.

Grayscale erosion with a flat disk shaped structuring element will generally darken the image. Bright regions surrounded by dark regions shrink in size, and dark regions surrounded by bright regions grow in size. Small bright spots in images will disappear as they are eroded away down to the surrounding intensity value, and small dark spots will become larger spots.

3.1.2 Dilation

Dilation is one of the two basic operators and is typically applied to binary images, but there are versions that work on grayscale images. The basic effect of the operator on a binary image is to gradually enlarge the boundaries of regions of foreground pixels (i.e. white pixels, typically) [27]. Thus areas of foreground pixels grow in size while holes within those regions become smaller.

To compute the dilation of a binary input image by a structuring element, we consider each of the background pixels in the input image in turn. For each background pixel (which we will call the input pixel) we superimpose the structuring element on top of the input image so that the origin of the structuring element coincides with the input pixel position. If at least one pixel in the structuring element coincides with a foreground pixel in the image underneath, then the input pixel is set to the foreground value. If all the corresponding pixels in the image are background pixels, the input pixel is left at the background value.

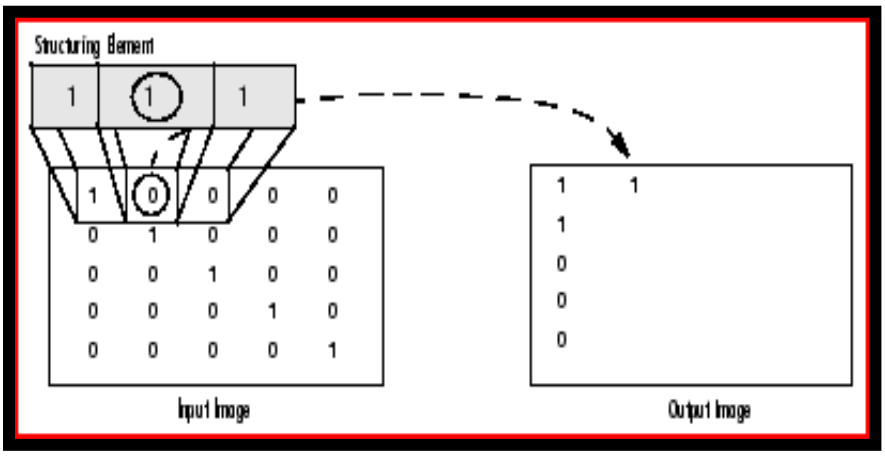

Figure 3.4. Effect of dilation using a 1×3 line structuring element.

In case of a 3×3 structuring element, the effect of this operation is shown in the Figure 3.5 (assuming 8 connectivity).

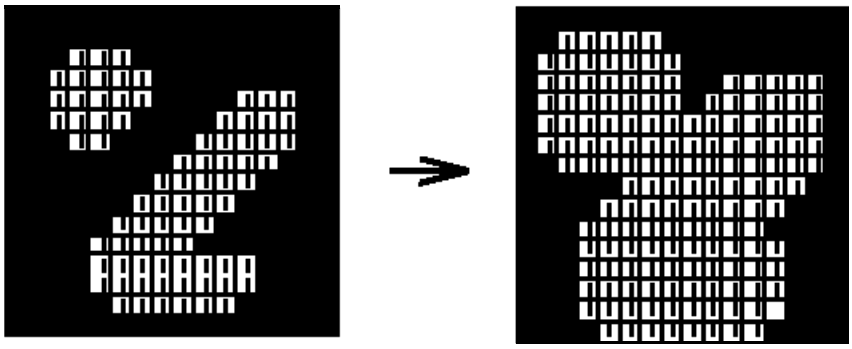

Figure 3.5. Effect of dilation using a 3×3 square structuring element.

Grayscale dilation with a flat disk shaped structuring element will generally brighten the image. Bright regions surrounded by dark regions grow in size, and dark regions surrounded by bright regions shrink in size. Small dark spots in images will disappear as they are `filled in' to the surrounding intensity value. Small bright spots will become larger spots. The effect is most marked at places in the image where the intensity changes rapidly and regions of fairly uniform intensity will be largely unchanged except at their edges.

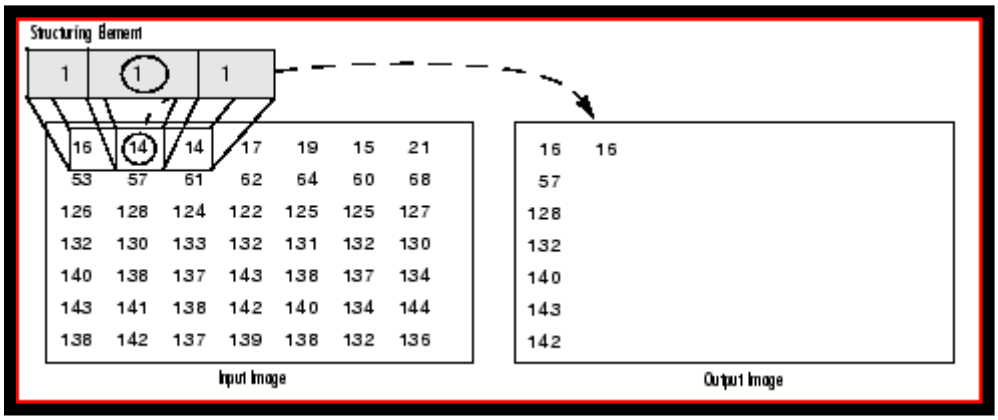

Figure 3.6. Grayscale dilation using a 1×3 line structuring element.

3.1.3 Opening and Closing

Opening and closing are two important operators from mathematical morphology. They are both derived from the fundamental operations of erosion and dilation. Like

those operators they are normally applied to binary images, although there are also gray level versions. The basic effect of an opening is somewhat like erosion in that it tends to remove some of the foreground (bright) pixels from the edges of regions of foreground pixels. However it is less destructive than erosion in general. As with other morphological operators, the exact operation is determined by a structuring element. The effect of the operator is to preserve foreground regions that have a similar shape to this structuring element, or that can completely contain the structuring element, while eliminating all other regions of foreground pixels [27].

Closing is an important operator and can be derived from the fundamental operations of erosion and dilation. Like those operators it is normally applied to binary images, although there are gray level versions. Closing is similar in some ways to dilation in that it tends to enlarge the boundaries of foreground (bright) regions in an image (and shrink background color holes in such regions), but it is less destructive of the original boundary shape. As with other morphological operators, the exact operation is determined by a structuring element. The effect of the operator is to preserve background regions that have a similar shape to this structuring element, or that can completely contain the structuring element, while eliminating all other regions of background.

3.2 Bit Plane Slicing

Pixel intensities are expressed as a combination of bits. In 8 bit gray scale image the intensities from 0 to 255 can be represented as binary combination of 8 bits. The 16 bit data of image contains 16 bit planes [27-29]. The intensities of the pixels can be decomposed into bit planes i.e. bit plane ‘1’ corresponding to bit ‘0’ (LSB) and so on up to bit plane ‘8’ (MSB or bit ‘7’). The most significant bit plane contains the visually significant data whereas the least significant bits give a coarse details/view of the image. The Figure 3.7 below shows the fact that as we move from the bit plane ‘1’ to bit plane ‘8’ the amount of information about the features is more significant in higher bit planes. Decomposing an image into bit planes gives a clear view of the contributions made by the each bit in the image.

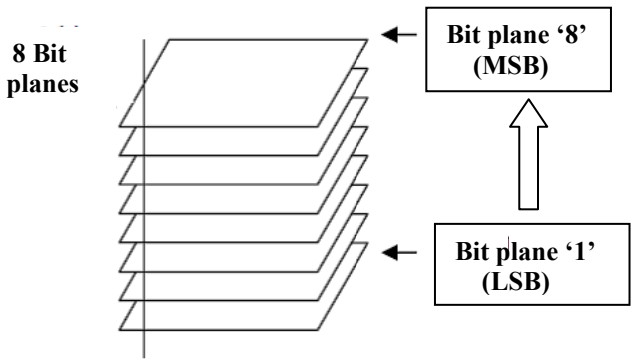

Figure 3.7. 8 Bit planes of a 8 bit data.

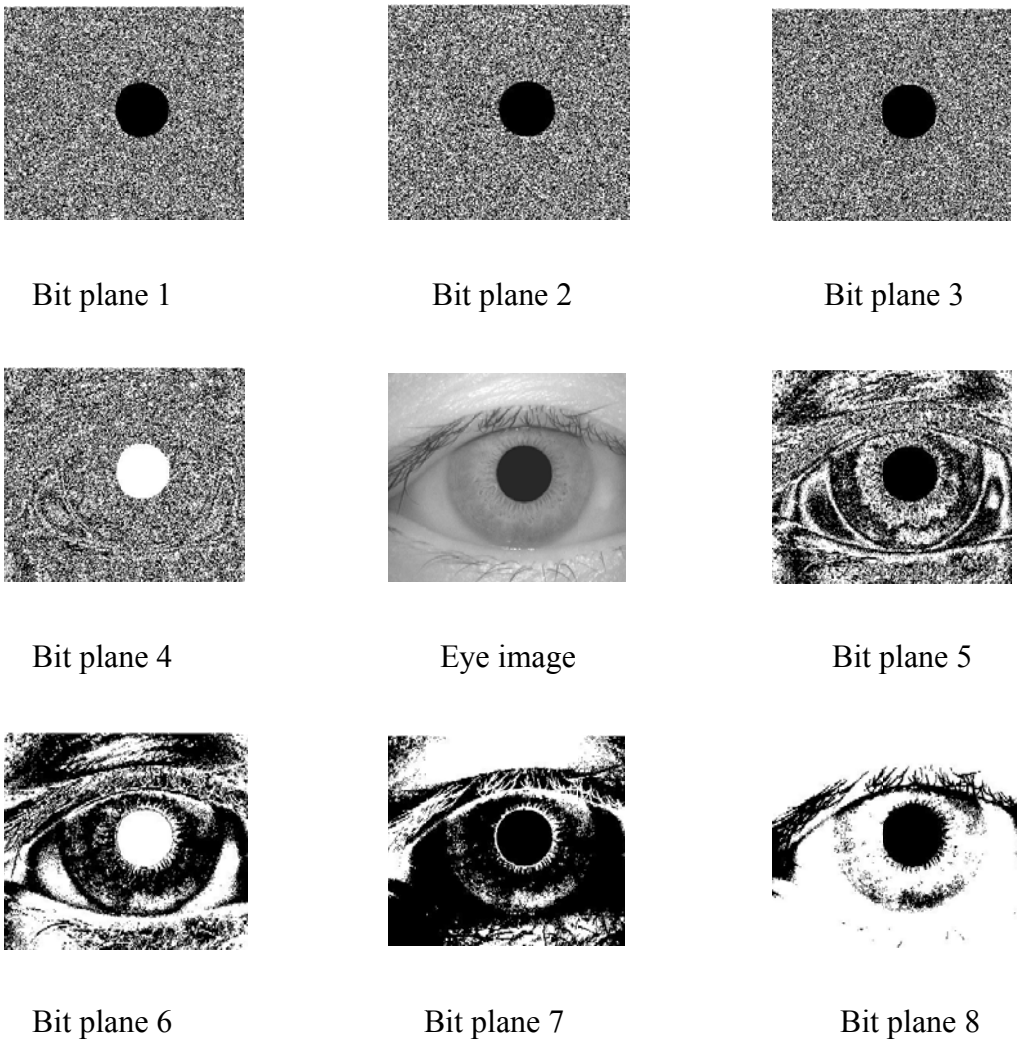

Figure 3.8. 8 Bit planes of an eye image – CASIA ver 1

3.3 Gaussian Blur

Gaussian filter is used as a low pass filter to blur an image in such a way that maximum weight is given to the centre pixel while decreasing the weight age of neighboring pixels in the final output. The filter has a bell shaped frequency response that makes it useful in smoothing as well as preserving the edges as compared to averaging filter.

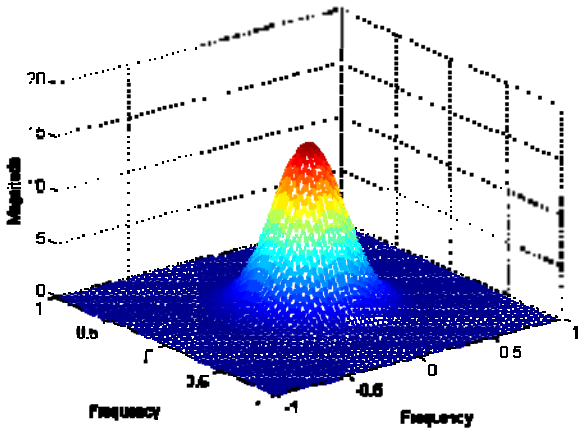

Figure 3.9. Frequency response of Gaussian filters.

The effect of Gaussian smoothing is to blur an image, in a similar fashion to the mean filter. The degree of smoothing is determined by the standard deviation of the Gaussian. Larger standard deviation Gaussians, of course, require larger convolution kernels in order to be accurately represented. The size of the kernel should normally be selected large enough so that the kernel coefficients of the border rows and columns contribute very little to the sum of coefficients. By selecting a kernel size parameters six times the standard deviation the border parameters will be 1% or lower than the center parameter.

3.4 Flow Chart of the Overall Proposed System

The flow chart of the complete proposed system is shown in Figure 3.10. The details of each stage will be covered in respective paragraphs during the discussion of implementation.

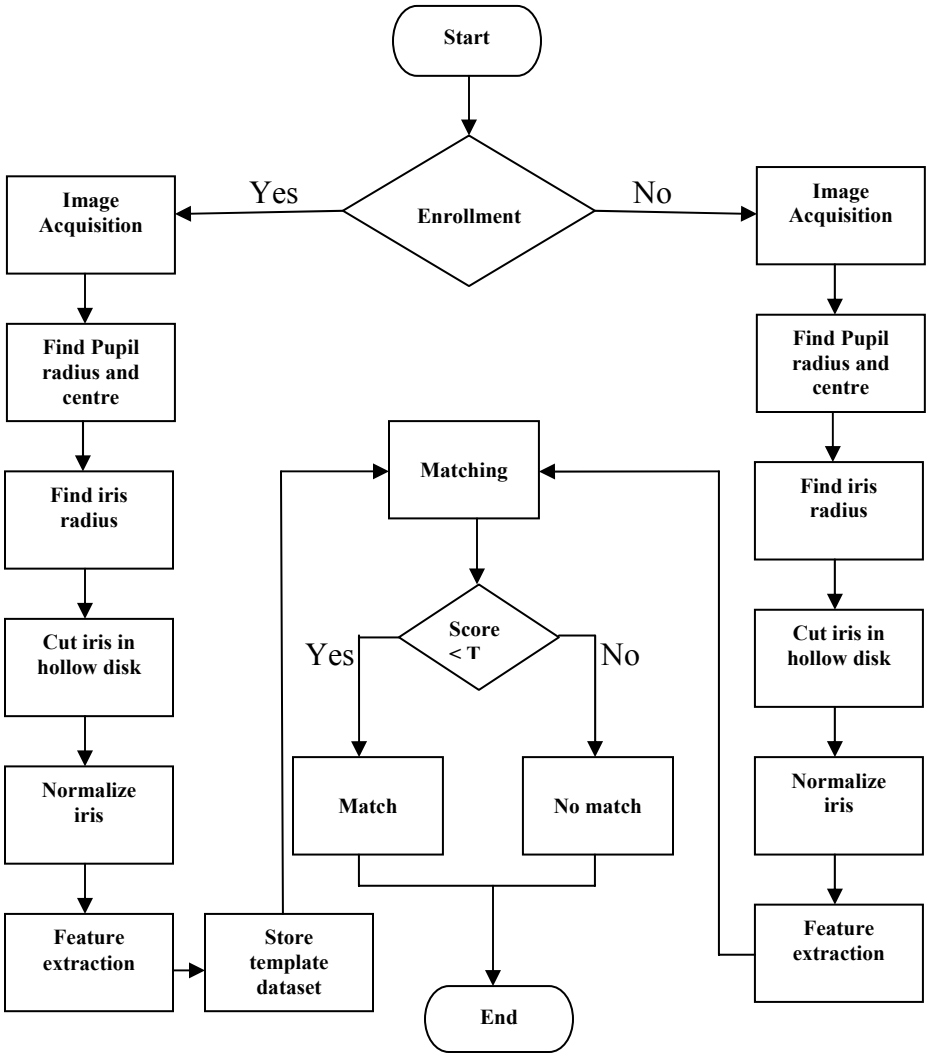

Figure 3.10. Flow chart of an overall system.

3.5 Iris Localization

The iris localization stage involves the detection of pupil boundary which is iris inner boundary and then finding the centre and radius of the pupil. In the second step the detection of the iris outer boundary is a difficult task as the contrast between the iris and sclera is very low. The iris and pupil both are approximated as circles with pupil taken as the centre. The pupil has been segmented as under:-

3.5.1 **Algorithm – 1** (using bit plane '1' and morphological operators)

The algorithm has been implemented without the use of edge detection.

- Extract bit plane '1' of the eye image as it gives the coarse information of the image.
- Complement the image obtained in step above, for image clean up by 'opening'.
- Morphological opening is performed to remove or suppress the isolated noise pixels and obtain a segmented pupil.
- Find the lowest (y_1) and highest (y_2) row numbers with non zero pixel (white pixel).
- Calculate the radius (r_1) of the pupil as under:-

$$r_1 = (y_2 - y_1)/2 \quad (2.16)$$

- Perform the step mentioned above to find the columns and find the radius (r_2) of pupil as under:-

$$r_2 = (x_2 - x_1)/2 \quad (2.17)$$

- Compare r_1 and r_2, the higher among the two will be the pupil radius.
- Find the centre coordinates by subtracting the pupil radius:-

$$c_y \text{ (row coordinate)} = y_2 - \text{pupil radius} \quad (2.18)$$

$$c_x \text{(column coordinate)} = x_2 - \text{pupil radius} \quad (2.19)$$

3.5.2 Algorithm 2 (Using bit plane '2' with canny edge detector and morphological operators) – (**The Proposed Algorithm**)

In Algorithm '1', the accuracy achieved is less as compared to the algorithm '2', which is more robust to high illumination and noise effects in the image, hence the same has been implemented.

- Extracting the bit plane '2' of the pupil for relatively sharp edges of pupil as compared to bit plane '1'.
- Performing the edge detection using Canny operator with value of sigma equal to '3' and applying adaptive threshold as under:-

$$T = \text{mean(Image)}/255 \quad (2.20)$$

- Find 8 connected objects in the edge detected image.
- If the number of objects in the image is '1', then find the pupil centre coordinates and radius using the procedure given in algorithm 1.

- If the number of objects is greater than '1', then perform morphological fill and erosion followed by dilation to clean the image and obtain a single white mass consisting of pupil.
- Perform the steps given in algorithm '1' above, to find the centre and radius of the pupil.

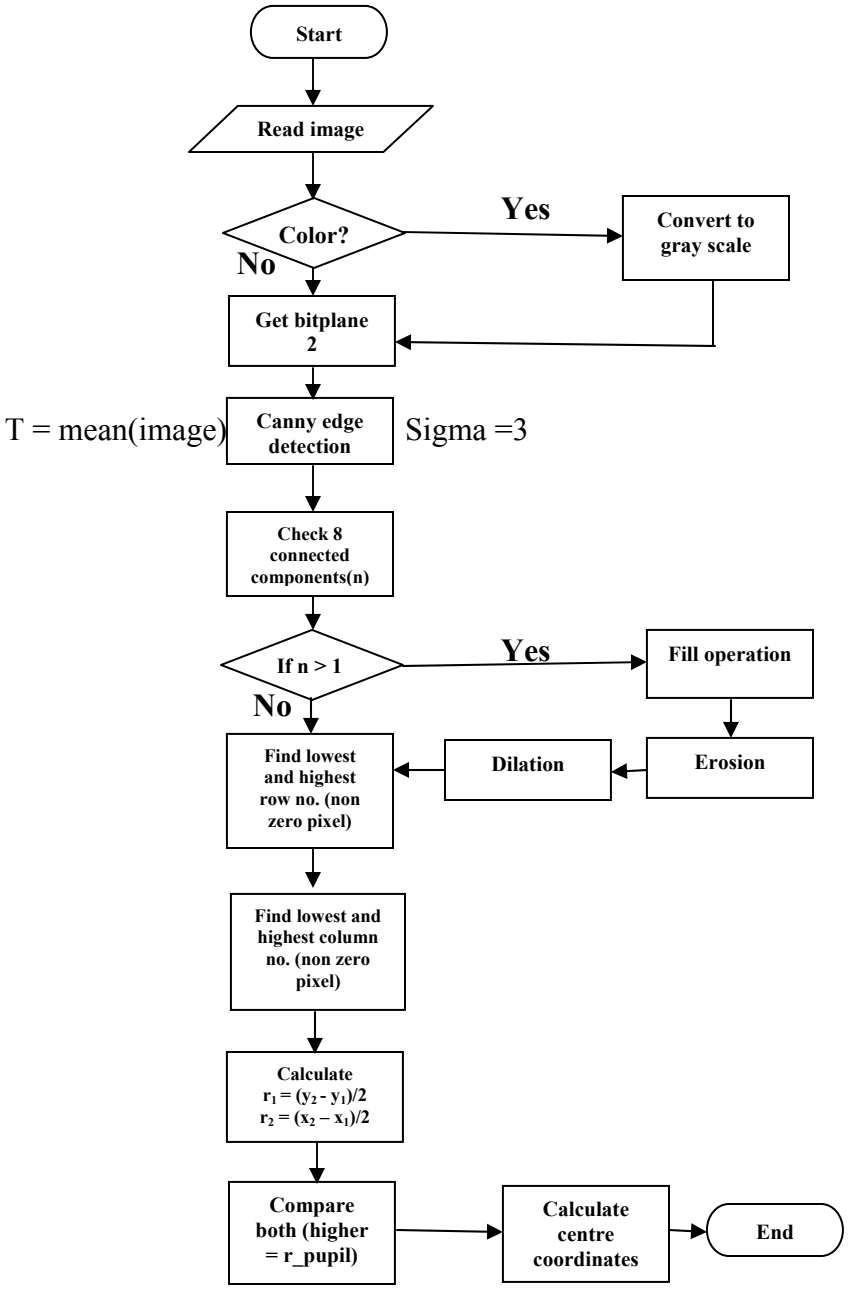

Figure 3.11. Flow chart of Pupil localization - (Algorithm 2)

3.5.3 Iris Outer Boundary Detection

Since the low contrast between the sclera and the iris is a major hurdle in the detection of the outer boundary therefore, few steps are required for pre-processing the image before going for its outer boundary detection.

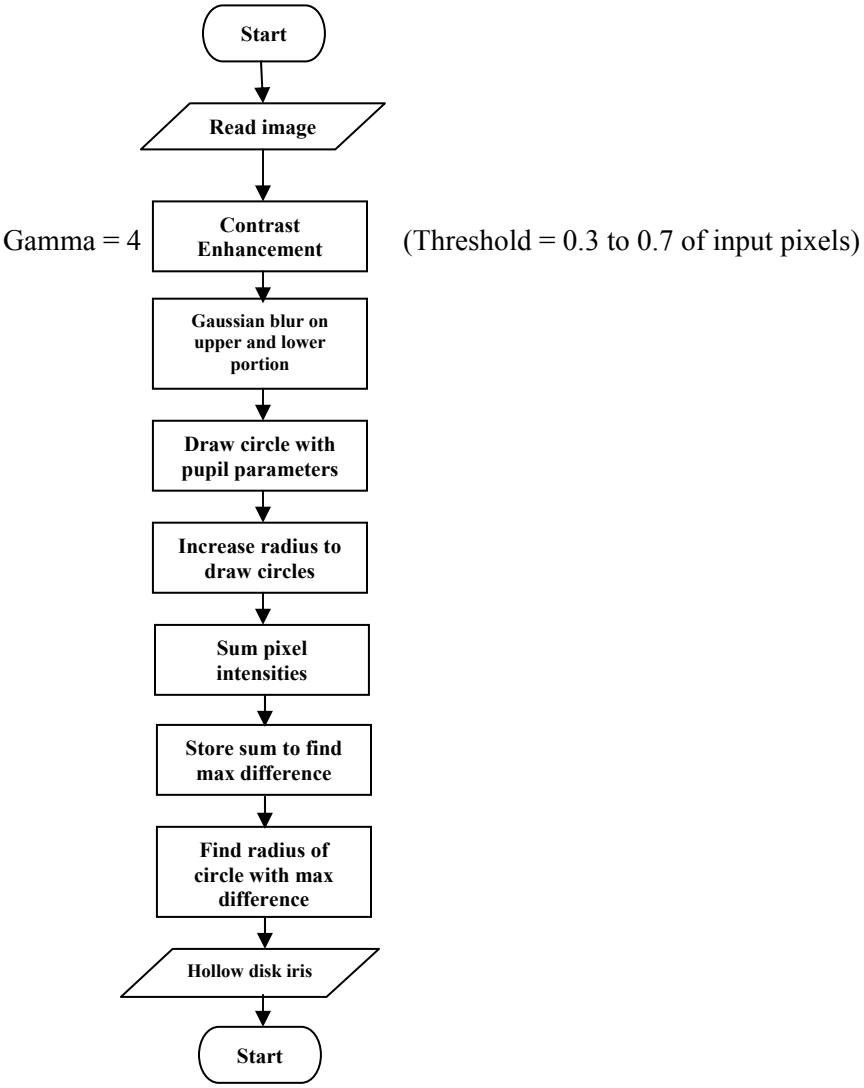

Figure 3.12. Flow chart of iris outer boundary detection.

Algorithm

- Carry out contrast enhancement to get the sharp boundary of the iris-sclera. The threshold of input pixel intensities has been adjusted between the values of 0.3 to 0.7 and the value of gamma equal to 4 has been selected.
- Apply the Gaussian blur to smooth the image for decreasing the effect of sharp edges in the upper and lower portion by masking the region of interest.
- Resize the image to avoid the circle search within the going beyond the specified limits in cases when the image is off centre too much on any one side.
- A Circle is used to represent the outer boundary that has the radius greater than the radius of the pupil.
- Taking the pupil centre and radius as initial parameters, draw a circle on the blurred image and sum the pixel intensities along the circumference of the circle.
- Pick only 360 x pixel intensities for the summation.
- Increase the radius by 1 pixel and keep drawing the circles at one pixel interval.
- Take the sum of pixel intensities on each circle and compare it with the previous sum. The circle having the maximum change in gradient will be the candidate for representing the outer boundary.
- Get the radius of circle and cut the iris in the doughnut shape.

3.6 Normalization of Iris

After the localization of iris, there is a need to compensate for the non linear varying size of the pupil and distance of the camera from the eye. For this purpose, iris is normalized using some reference point and thus the pupil centre is used. This unwrapping makes the computation easier in a row column format.

3.6.1 Rubber Sheet Model

The pupil and iris are assumed to be eccentric having the same centre coordinates and conversion from the Cartesian to polar coordinates is carried out using the equations

given below. The radial resolution for rows is set to 64 and angular resolution for columns is 180 pixels in case of normalized image. If the width of iris is 32 pixels then every pixel will be picked twice, similarly, if the width of iris is 128 pixels then every second pixel will be discarded to make 64 rows [1]. The points in the iris region are remapped in the interval [0, 1] and angle [-π/4, 5π/4] in clockwise direction. In the Figure 3.13, r is the number of points along radius and θ is the angular resolution. Polar coordinates (r, θ) are dimensionless.

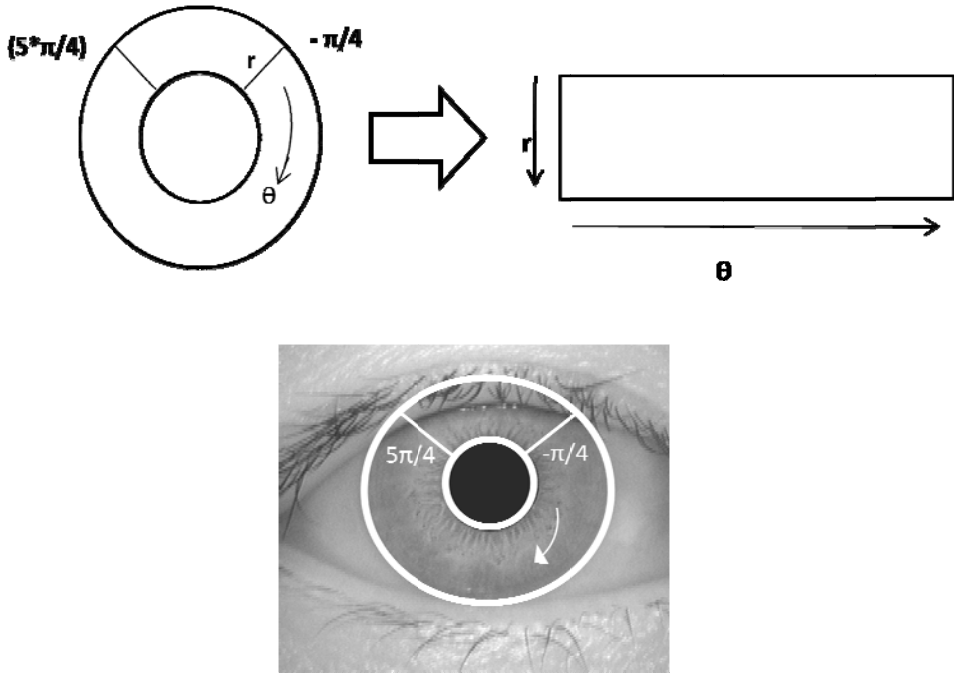

Figure 3.13. Normalization method

(2.21)

(2.22)

where

In the radial direction, the texture is assumed to change linearly, which is known as the rubber sheet model. The upper part of the eye is usually occluded by the upper eyelids so interval between 45 to 135 degrees is not considered for normalization of iris region. This has the advantage of avoiding the occlusion caused by the upper eyelids but a disadvantage of losing some information in this region. However, the results obtained by the algorithm are superior to many techniques when compared.

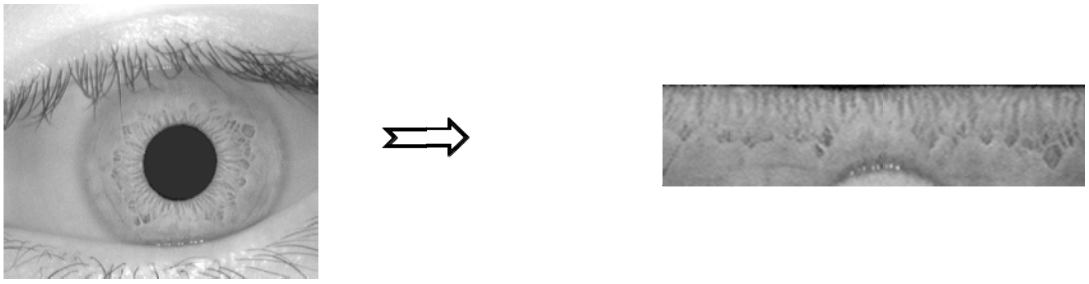

Figure 3.14. Normalized image of size 64*180.

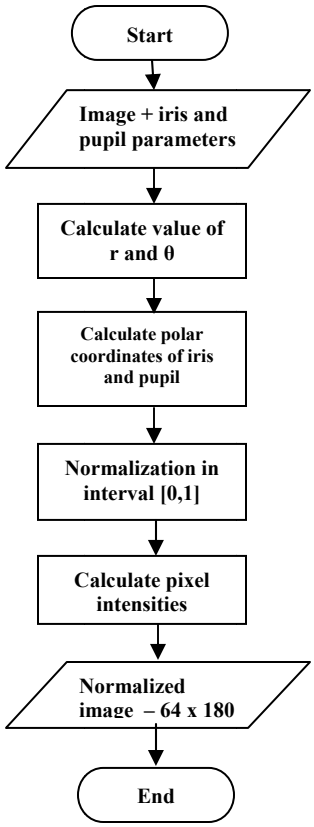

Figure 3.15. Flow chart of normalization algorithm.

3.7 Feature Extraction using Bit Plane Slicing

Discriminating features from the normalized image are required to be extracted for the matching purpose. Bit plane slicing is used and it can be seen in the figures below that the most discriminating information in this case, is present in bit plane 5, 6 and 7 because normalized image contains the middle frequencies (pixel intensity levels) only, whereas it has been proved in the available literature that significant data of the image is present in bit plane '8' (MSB). In this case, bit planes 1, 2, 3, 4 and 8 are not considered for the feature extraction. I have used the MATLAB in built function, '*bitget*', to extract the bit planes of the images. The two input arguments to this function are, an unsigned integer array and the number of bit planes from '1' to '8' (for grayscale 8 bit image only) required to be extracted in 256 level gray scale image.

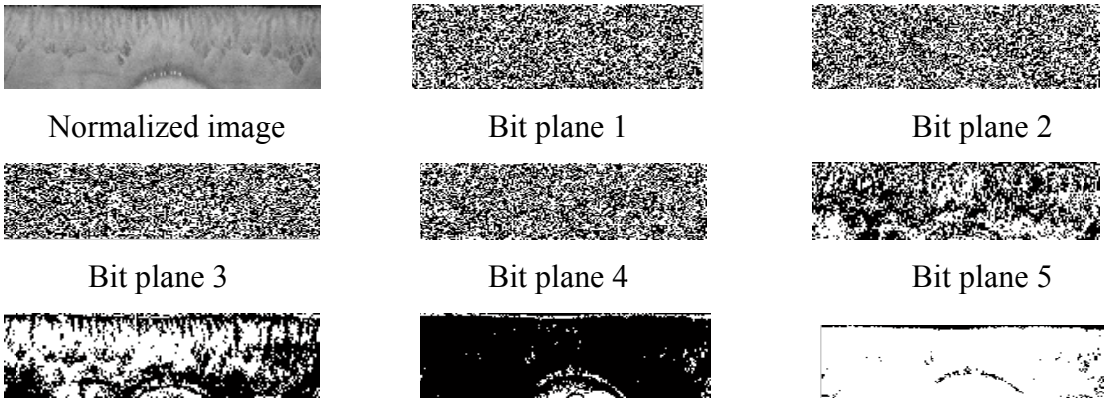

Figure 3.16. Bit planes of a normalized image.

3.8 Matching

Once the features have been extracted from the iris images, then in order to find a match, a measure of similarity between the subject and stored template is required. This can be accomplished by calculating the hamming distance between the two binary templates. This matching metric should be able to provide a distinct and a clear separate score for the intra and inter class comparisons.

3.8.1 Matching by Hamming Distance

The Hamming distance gives a measure of how many bits are the same between two bit patterns. Using the Hamming distance of two bit patterns, a decision can be made as to whether the two patterns were generated from different irises or from the same one. In comparing the bit patterns *X* and *Y*, the Hamming distance, *HD*, is defined as the sum of disagreeing bits (sum of the exclusive-OR between *X* and *Y*) over *N*, the total number of bits in the bit pattern.

$$HD = \frac{1}{N} \times \sum_{i=1}^{N} X_i \, (XOR) Y_i \qquad (2.23)$$

Since an individual iris region contains features with high degrees of freedom, each iris region will produce a bit-pattern which is independent to that produced by another iris, on the other hand, two iris codes produced from the same iris will be highly correlated. If two bits patterns are completely independent, such as iris templates generated from different irises, the Hamming distance between the two patterns should equal 0.5. This occurs because independence implies the two bit patterns will be totally random, so there is 0.5 chance of setting any bit to 1, and vice versa. Therefore, half of the bits will agree and half will disagree between the two patterns. If two patterns are derived from the same iris, the Hamming distance between them will be close to 0, since they are highly correlated and the bits should agree between the two iris codes. The Hamming distance is the matching metric employed by Daugman, and calculation of the Hamming distance is taken only with bits that are generated from the actual iris region.

CHAPTER 4

IMPLEMENTATION AND RESULTS

4.1 Image Dataset

The proposed system has been implemented in the MATLAB version 7.6 installed on 1.8 GHz system with 1 GB RAM. The experiments were conducted on the CASIA version 1 which is publicly available for research work. There are a total of 756 images from 108 subjects. The images have been captured in two sessions, session I contains 3 x images per subject and session II contains 4 x images per subject. The details of the implementation and results are discussed in the succeeding paragraphs.

4.2 Pupil Localization

Pupil localization has been implemented using the two algorithms. Algorithm two has proved to be more robust and accurate for the pupil detection and finding pupil parameters. The approach was to first isolate the pupil, the dark portion in the center of the eye. The pupil was isolated using bit-plane processing. The pupil appeared as a large homogenous region surrounded by insignificant noise which allowed for easy definition of the pupil-iris boundary.

4.2.1 Algorithm '1'

In this case canny edge detector has been used and bit plane '1' along with the morphological opening has been applied to localize the pupil. I have extracted the bit plane '1' using 'bitget' function and image clean up has been done by taking the complement of image and morphological opening by using a disk type structuring element of radius equal to 9. When the pupil is isolated, module 'pupil_para' is called to give the radius and centre of the pupil.

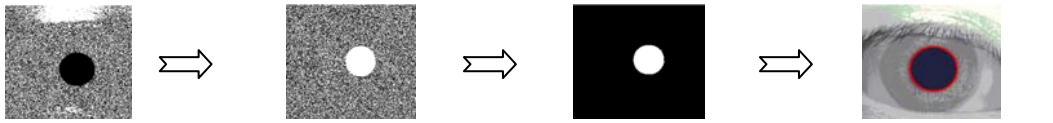

Figure 4.1. Steps for pupil localization

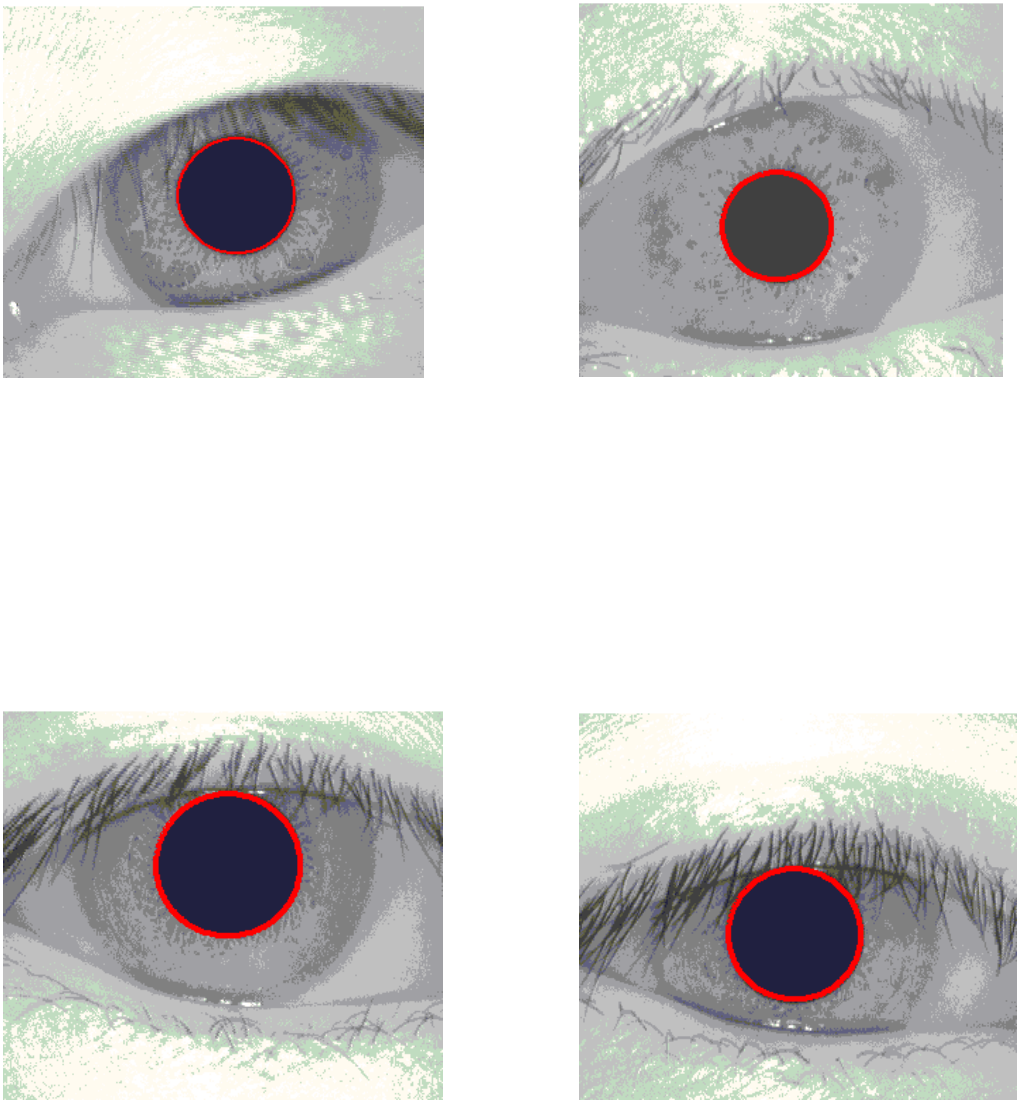

Figure 4.2. Examples of few correctly localized pupils.

4.2.2 Algorithm '2' (Proposed)

Since the results obtained in the first case are 97.1 %, due to sensitivity of the morphological operators to noise. A more robust algorithm is used in the implementation and discussed here. Canny edge detection with value of sigma '3' and adaptive threshold is used in combination with bit plane '2' and morphological operators. Bit plane '2' gives a little sharp edges of the pupil than bit plane '1'. Canny edge detector is used to detect the edge of pupil with value of sigma equal to '3' and threshold selected as the mean of the pixel intensities of an input image. Check 8 connected components in the image using 'bwlabel' function. If the number of objects is one, module 'pupil_para' is called otherwise in order to isolate the pupil, use morphological filling, erosion and dilation in conjunction with a suitable structuring element. A disk type structuring element with a radius equal to '9' has been used. Then call 'pupil_para' to find parameters and draw the circle on pupil boundary.

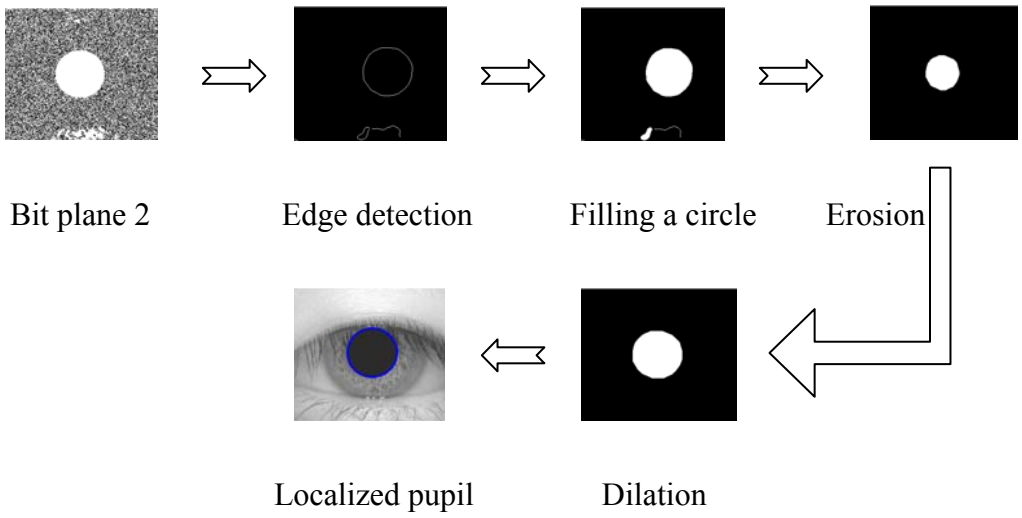

Figure 4.3. Steps for pupil localization –Algorithm 2

The figure 4.4 shows few cases of exact localization of pupil.

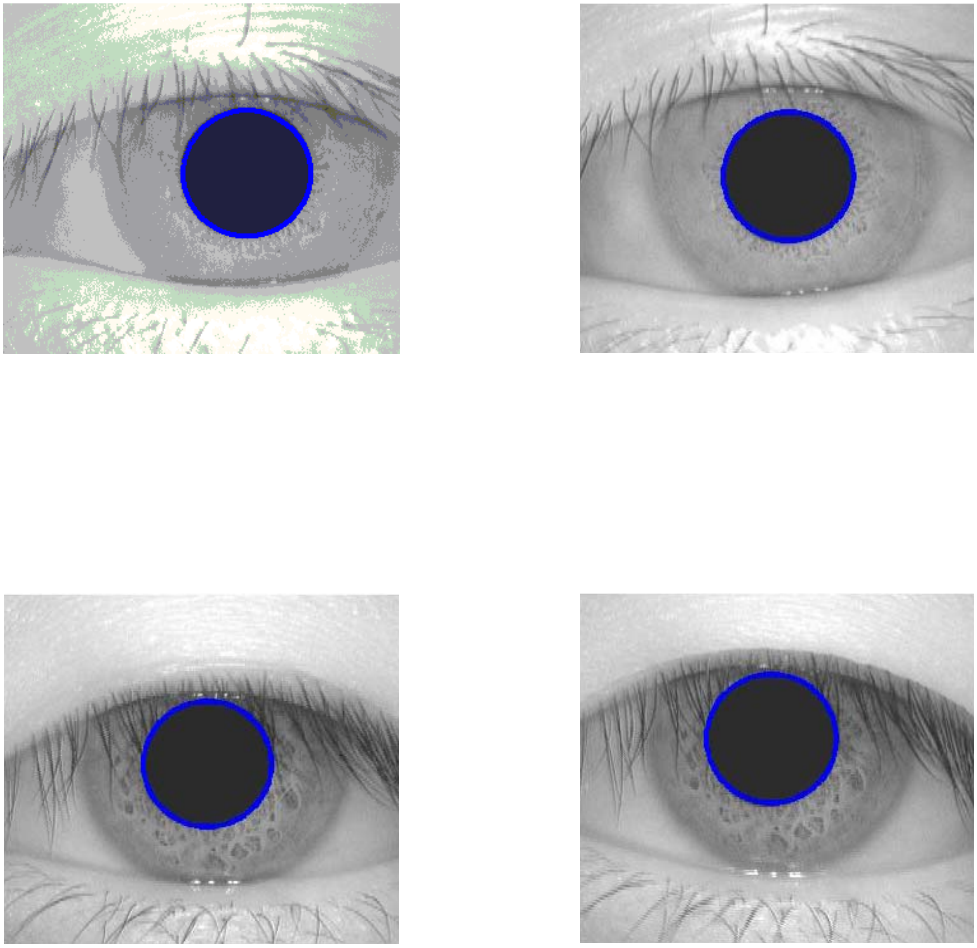

Figure 4.4. Examples of few correctly localized pupils - Algorithm 2.

4.3 Iris Outer Boundary Detection

The outer boundary detection starts with contrast enhancement by adjusting the values of input pixel intensities between threshold values of 0.3 to 0.7 and selecting value of gamma equal to 4. Gaussian blur of window size 50 * 50, with sigma equal to '3', is applied to smooth the upper and lower part of the image because the upper and lower eyelids present strong edges. These edges will negatively affect the detection of the iris boundary by circular summation which is used to detect the maximum difference. Masking is used to select the upper and lower portions. The upper portion starts from row one and ends at the edge of the pupil upper boundary. The lower portion starts from the lower boundary of the pupil and ends at the last row. This technique helps in preserving

about 50% of the sharp edges of iris-sclera boundary on the right and left sides as shown in the Figure 4.5.

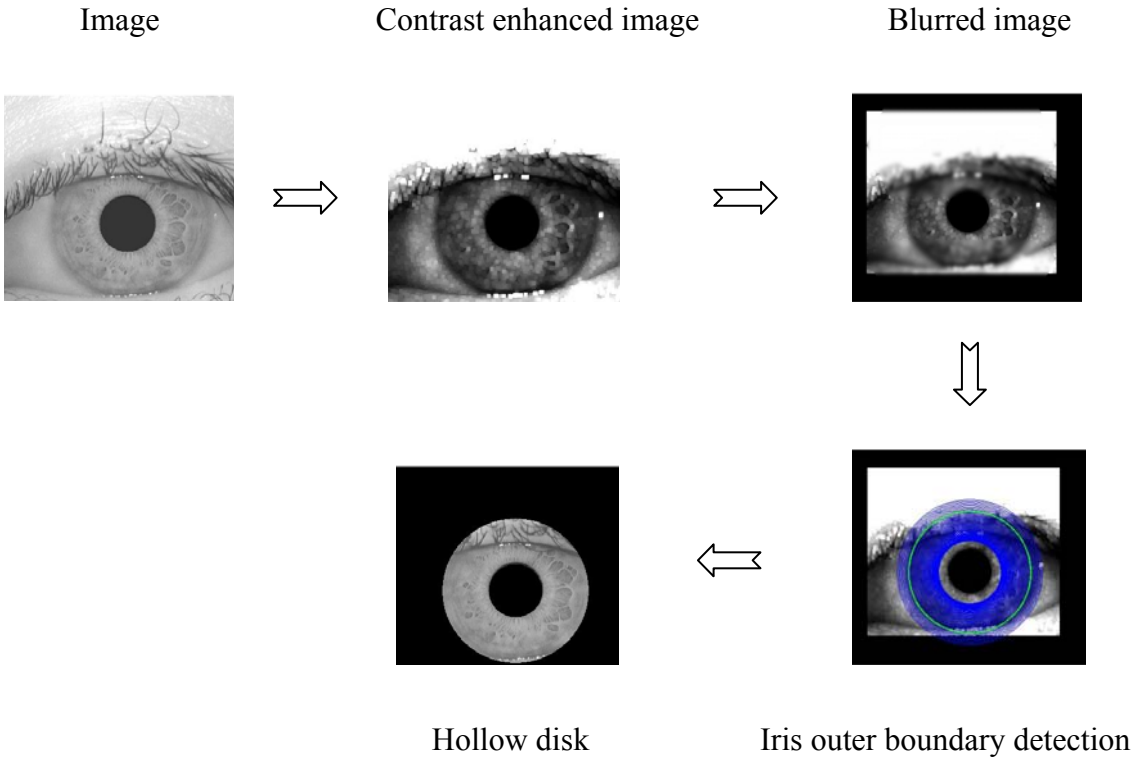

Figure 4.5. Steps for iris localization.

Initially, by considering the parameters of a pupil draw a circle on the image and sum up 360 samples of pixel intensities on the circumference of the circle. Increment the radius by one pixel and draw another circle to get the sum. Get the difference of two and keep on increasing the radius until a circle with maximum difference is obtained which is the candidate circle for representing the iris boundary. The parameters of the iris are confirmed and iris is cut in the form of a hollow disk. Hence, the iris effective region is localized in an efficient and accurate manner. The hollow disk type iris is required to be normalized for carrying out the comparison between the iris images of same eye which are captured under different conditions.

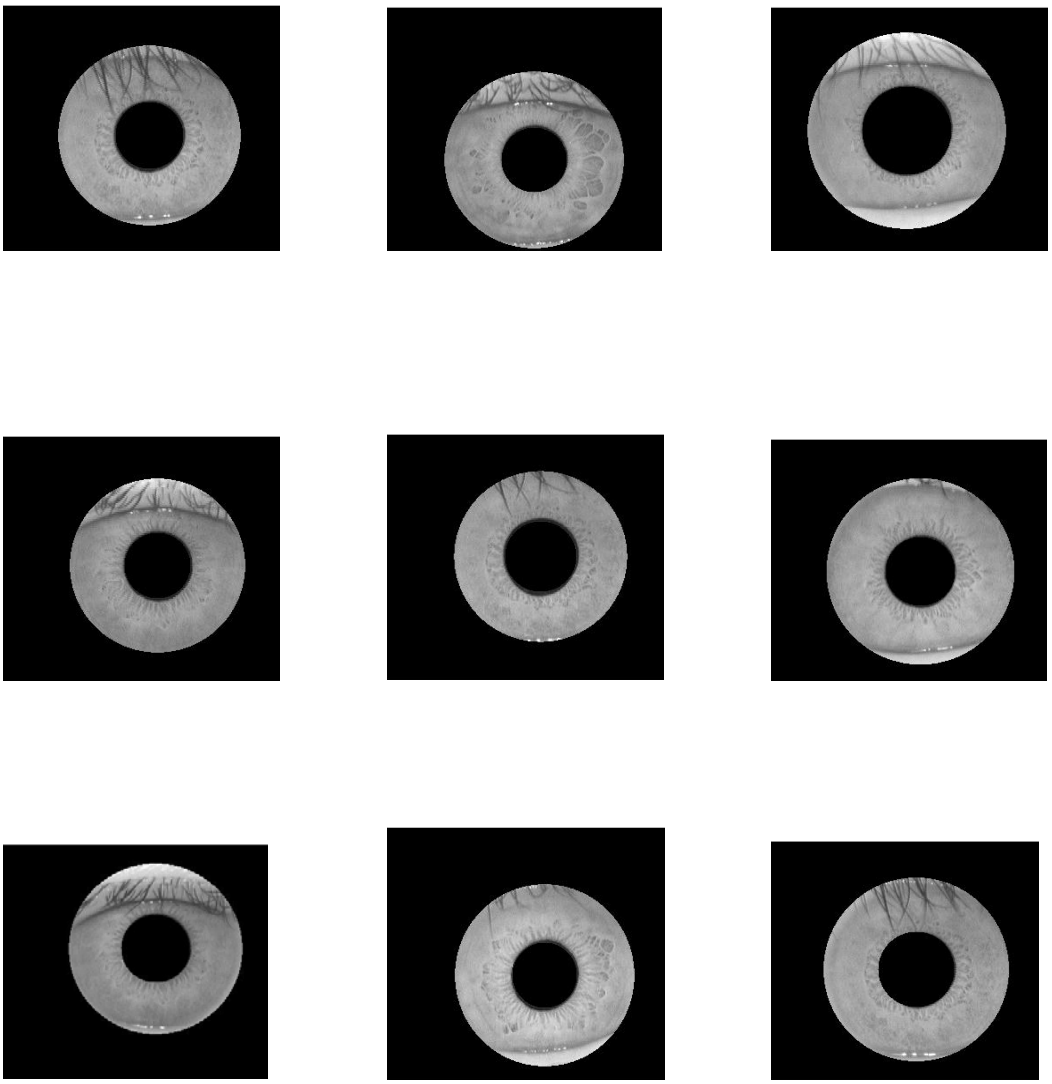

Figure 4.6. Few examples of iris localization.

4.4 Normalization

4.4.1 Daugman's Method

The normalization has been carried out by calling the module '**rubber_sheet**'. The size of the normalized image is kept 64 x 180 for the optimum results. Notice the large eyelid regions at the top and bottom of the image. These are the areas inside the iris circle that are covered by an eyelid. These regions do not contain any useful data and need to be discarded. One way to do this is to detect regions of the image that are

unneeded and note the position of pixels within the region. Then, when the iris pattern is decoded and compared to another image, only regions that are marked "useful" in both images are considered.

The value of r is equal to 64 and value of θ is selected as 180 between the interval $-\pi/4$ to $5\pi/4$ in the clockwise direction. The upper region of $\pi/2$ (90 degrees) has not been considered because of upper eyelid occlusions. This technique has an advantage of ignoring a major source of occlusions but also has a disadvantage of losing some information useful for matching. However, results found are superior to the other techniques.

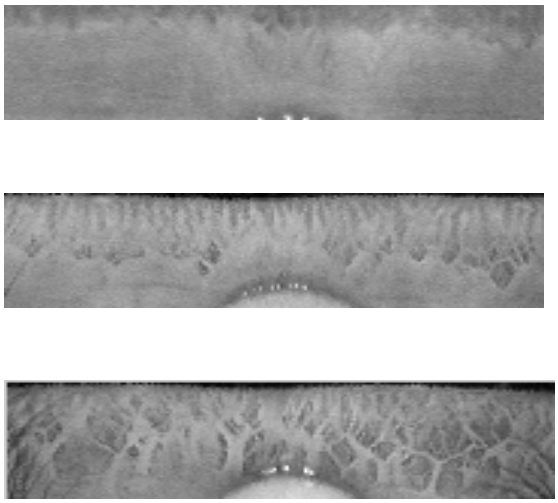

Figure 4.7. Few examples of iris normalization by Rubber sheet model**.**

(Size 64x180)

4.5 Feature Extraction

Bit plane 5, 6 and 7 are used for the feature extraction using the MATLAB function 'bitget'. The extracted bit planes are used to check the recognition rate by using the normalized hamming distance. Figure 4.8 shows the information about the iris texture which is available in each bit plane. It has been proved in [1] that the most discriminating

features are present in bit plane 5 of the normalized image. Feature vectors are extracted using a straight forward and swift method.

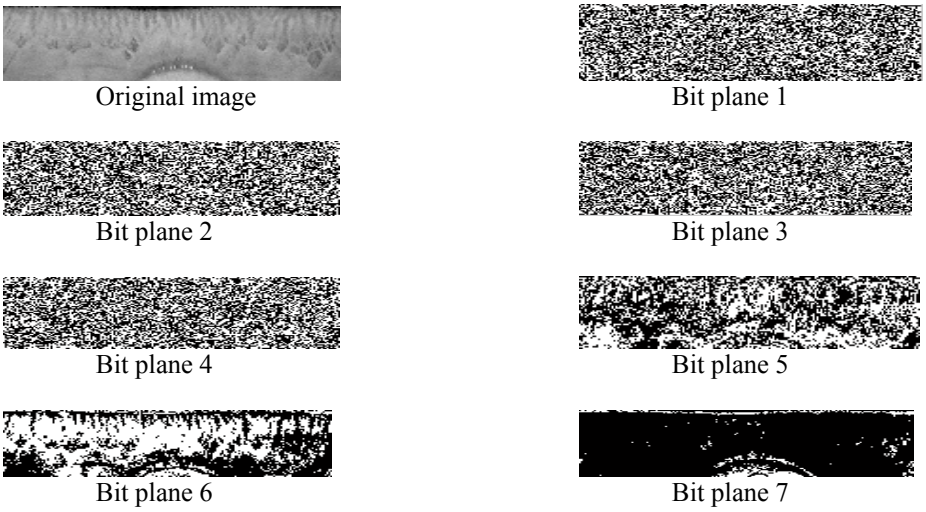

Figure 4.8. Bit planes of a normalized image.

4.6 Results and Analysis

In the previous sections, the procedure of implementation is explained thoroughly. The iris pre-processing is performed to detect the iris region in the human eye. After the normalization and feature extraction of the iris, the system is tested upon the inputs. In CASIA version 1 [31], there is total of 756 gray scale images of size 280 x 320.

4.6.1 Pupil Detection

The proposed algorithm obtained 100% accuracy in the detection of the pupil and parameters have been found correctly. Irrespective of the techniques used, the comparison of the accuracy of the algorithm with other methods is given in Figure 4. Average time required for detecting the pupil on a 1.8 GHz, 1 GB RAM is 0.228 seconds.

Table 4.1. Pupil localization results

Method	Accuracy
Mehrabian et al	100%
Hough Transform	97.48%
Narote et al	100%
Masek	99.07%
A. Basit	100%
Proposed	100%

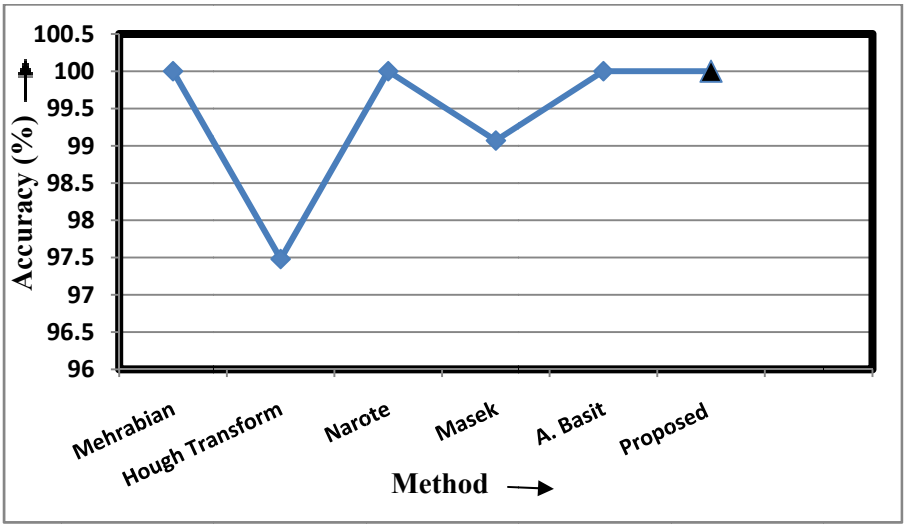

Figure 4.9. Pupil localization - accuracy comparison.

4.6.2 Iris Localization

After successfully localizing the pupil in all 756 images, I implemented the iris localization method in which only 4 x images were not correctly localized and this gave an accuracy of 99.47%. Irrespective of the techniques used, results of time consumed and comparison with the other algorithms show that the performance achieved in time as well as accuracy is optimum.

Method	Accuracy	Min Time	Min Time	Avg Time
Daugman	98.6%	6.23	6.99	6.56
Wildes	99.90%	6.34	12.54	8.28
Masek	82.54%	6.3	43.3	17.5
A. Basit	99.60%	0.33	0.24	0.41
Proposed	99.47%	0.507	0.873	0.52

Table 4.2. Iris localization results.

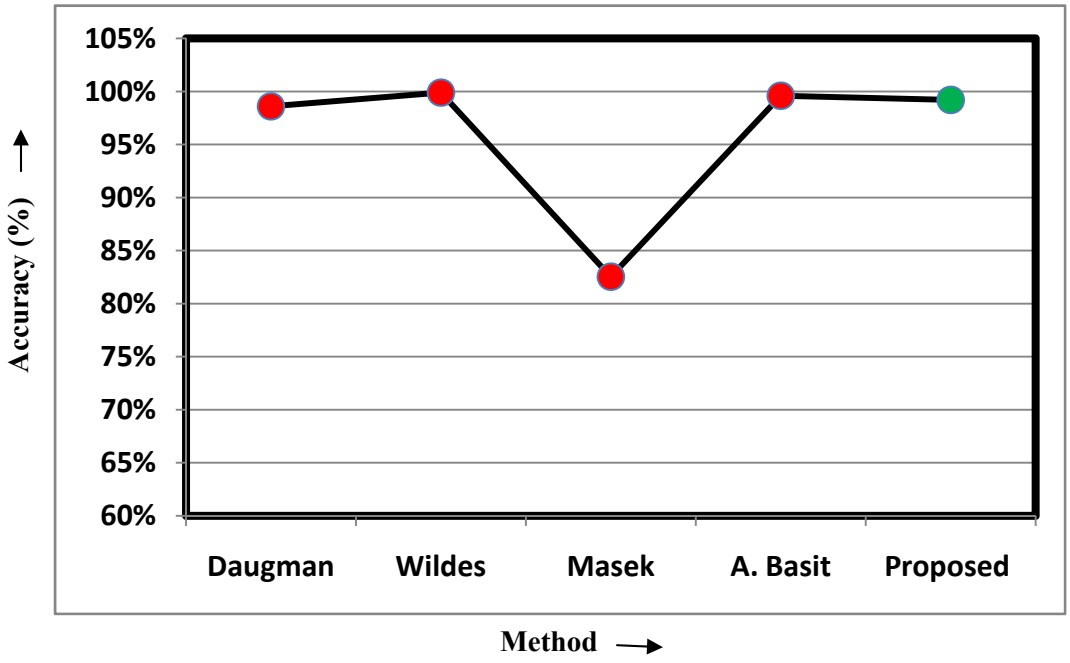

Figure 4.10. Iris Localization accuracy comparison.

4.6.3 Normalization

Normalization is carried out using Daugman's rubber sheet method and the results obtained are tabulated in the Table 4.3. Pupil centre has been taken as the reference point

in both cases but the techniques to find the parameters differ in both cases. Advantage of time saving has been achieved in the proposed method.

Table 4.3. Time comparison of normalization

Method	**Min Time (secs)**	**Max Time (secs)**	**Average Time (secs)**
A. Basit	Not mentioned	Not mentioned	0.05
Implemented	0.0204	0.0376	0.0219

4.6.4 Experiments

Five experiments have been conducted to check the recognition rate of bit plane 5, 6 and 7 only. The numbers of enrolled images have been increased while keeping the number of test images constant and same in all experiments.

2.6.4.1 Scenario 1

Implemented algorithm takes 1 x training image each of 100 subjects as input, whereas there are a maximum of seven images for each subject. Total number of enrolled images is 100 from session II and image 3 of the session I of l00 subjects has been selected as test image. Thus, a total number of test images is 100, after testing I obtained the following results.

Table 4.4. Recognition rate of bit planes – experiment 1.

Number of enrolled images	Number of test images	Correct recognition rate of test images		
		Bit plane 5	Bit plane 6	Bit plane 7
100	100	75%	84%	51%

The following Figure 4.11 displays the testing results in which the input images are compared with all the templates in the database.

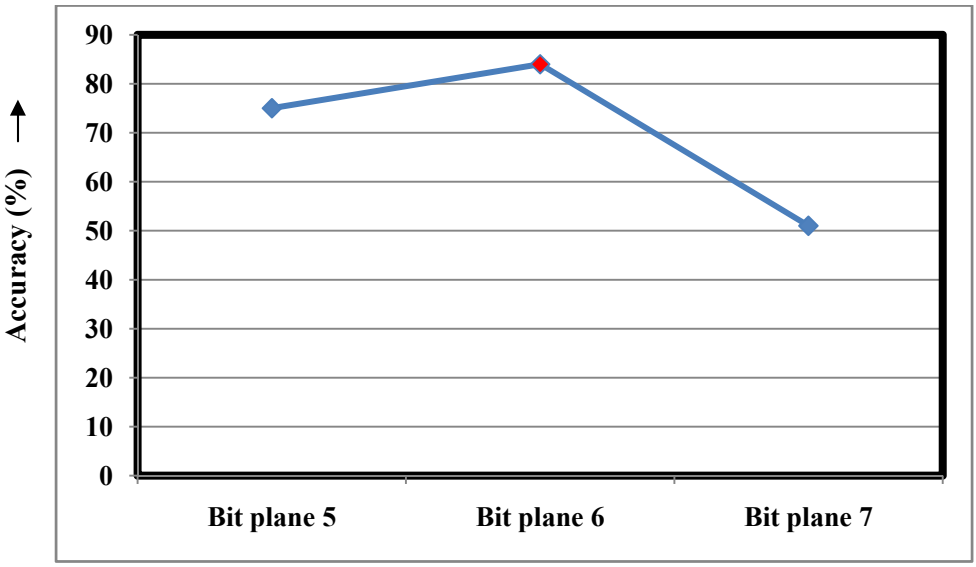

Figure 4.11. Results of experiment 1.

4.6.4.2 Scenario – 2

The implemented algorithm takes 100 subjects with 2 x training images each as input from the session II, hence, number of enrolled images is 200 and test images are the same as in scenario 1. After testing I obtained the following results.

Table 4.5. Recognition rate of bit planes – experiment 2.

Number of enrolled images	Number of test images	Correct recognition rate of test images		
		Bit plane 5	Bit plane 6	Bit plane 7
200	100	83%	92%	53%

The following Figure 4.12 displays the testing results in which the input images are compared with all the templates in the database. Bit plane '6' has the highest recognition rate as compared to bit plane 5 and 7 in both the experiments.

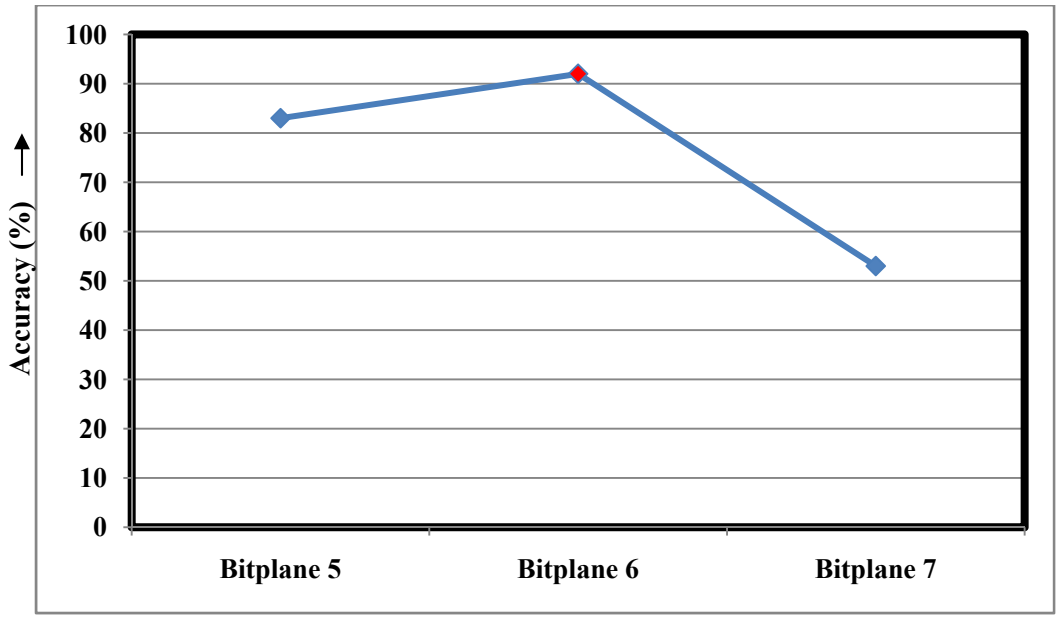

Figure 4.12. Results of experiment 2.

4.6.4.3 Scenario – 3

Implemented algorithm takes 100 subjects with 3 x training images as input from session II whereas number of test images is again kept the same as in the previous two cases. After testing I obtained the following results.

Table 4.6. Recognition rate of bit planes – experiment 3.

Number of enrolled images	Number of test images	Correct recognition rate of test images		
		Bit plane 5	Bit plane 6	Bit plane 7
300	100	87%	91%	65%

The following Figure 4.13 displays the testing results in which the input images are compared with all the templates in the database. The recognition rate in case of bit plane 6 has decreased from 92 to 91 percent.

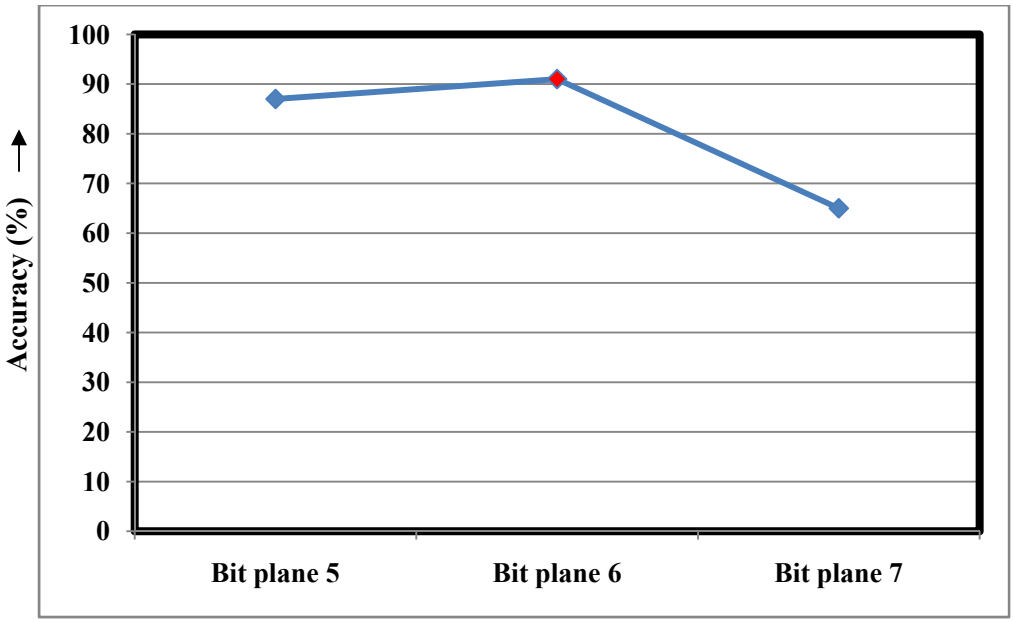

Figure 4.13 Results of experiment 3.

4.6.4.4 Scenario – 4

Implemented algorithm takes 100 subjects with 4 x images each as input, making a total number of test images as 400, after testing I obtained the following results.

Table 4.7. Recognition rate of bit planes – experiment 4.

Number of enrolled images	Number of test images	Correct recognition rate of test images		
		Bit plane 5	Bit plane 6	Bit plane 7
400	100	91%	94%	72%

The following Figure 4.14 displays the testing results in which the input images are compared with all the templates in the database.

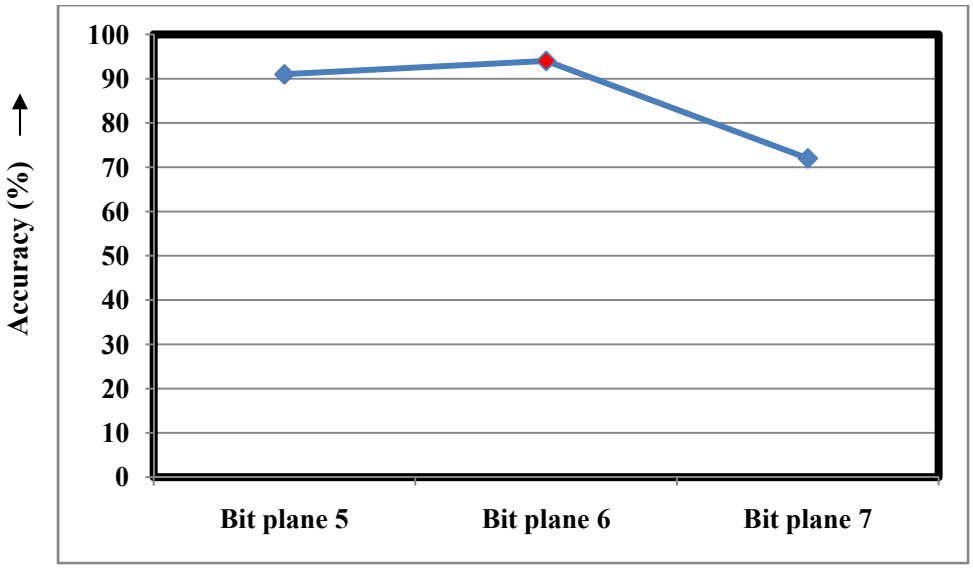

Figure 4.14. Results of experiment 4.

4.6.4.5 Scenario – 5

Implemented algorithm takes 500 enrolled images including 4 x images of session II and the 5th image is taken as the average of the 4 x images of session II. The tests showed the results as tabulated below and shown in the Figure 4.15. The highest recognition is 98% in case of bit plane 6.

Table 4.8. Recognition rate of bit planes – experiment 5.

Number of enrolled images	Number of test images	Correct recognition rate of test images		
		Bit plane 5	Bit plane 6	Bit plane 7
500	100	92%	98%	81%

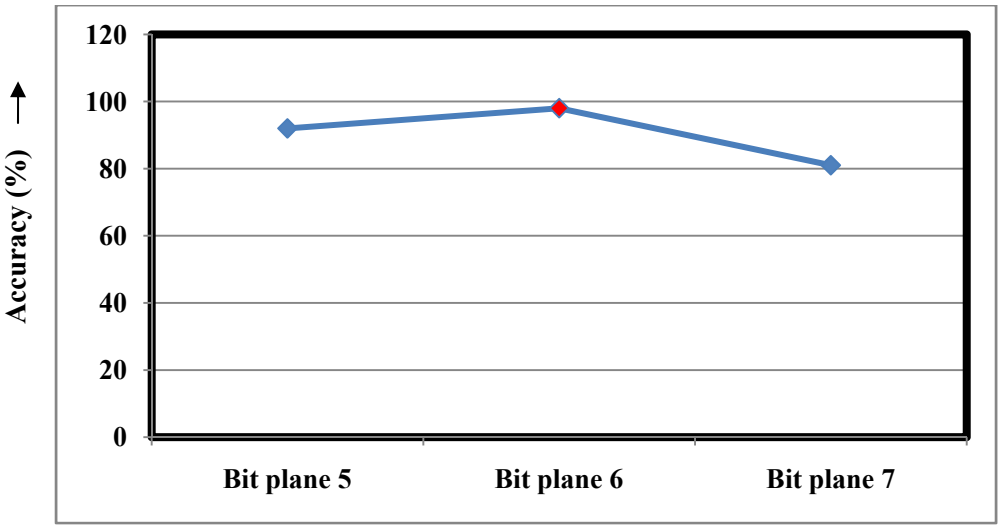

Figure 4.15. Results of experiment 5.

4.6.5 Comparison of Bit Planes

After carrying out the comparison of all scenarios mentioned above, the best matching result the features is obtained in case of bit plane 6 which shows correct recognition rate of 98%. The graph also shows that the correct recognition rate increases with the increase in the number of enrolled images.

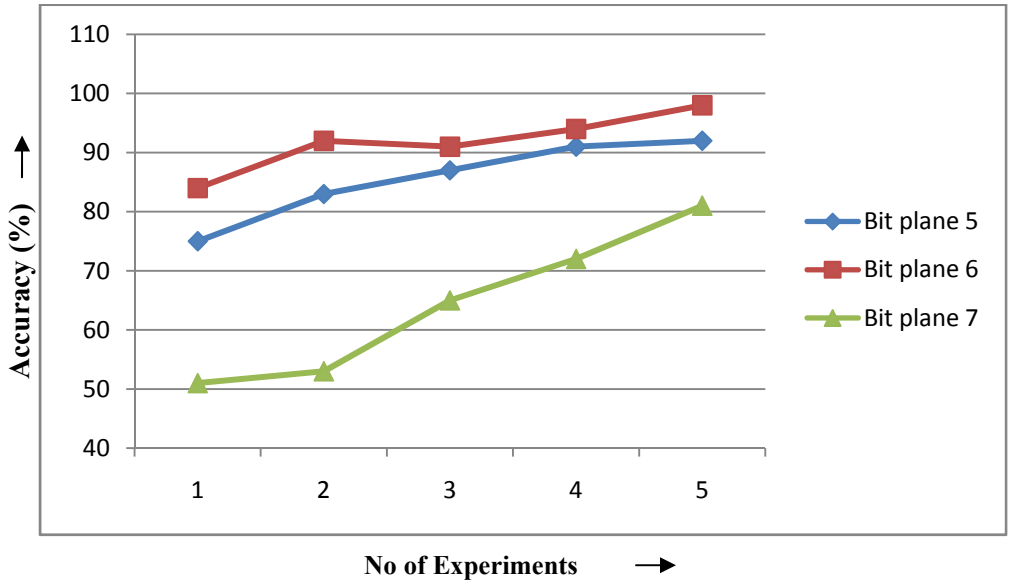

Figure 4.16. Comparison of results of bit planes.

4.6.6 Comparison of Results with Other Iris Recognition Methods

The algorithm has been implemented using 1.8 GHZ Intel Centrino machine with Windows Vista and MATLAB 7.6 as the development tool. This section compares results of my proposed technique with the other techniques which have been implemented on the same dataset i.e., CASIA version 1.

The comparison of the time required for extracting the features and matching stage is shown in the Table 4.9. The Figure 4.17 provides a pictorial analysis of the time comparison which shows that the implemented technique has gained benefits on all other techniques in terms of the time required for computations during the feature extraction and matching stages. The total time spent in both stages is only 1.8 milliseconds. The feature extraction method is fast enough to spend only 90 micro seconds.

Table 4.9. Time comparison – feature extraction and matching

Method	Feature Extraction Time (ms)	Matching Time (ms)	Total Time (ms)
Daugman	422	31	453
Tan	125	68	193
Monro (DCT)	30	31	61
A. Basit (Wavelets)	Not mentioned	Not mentioned	70
Proposed	0.09	1.71	1.8

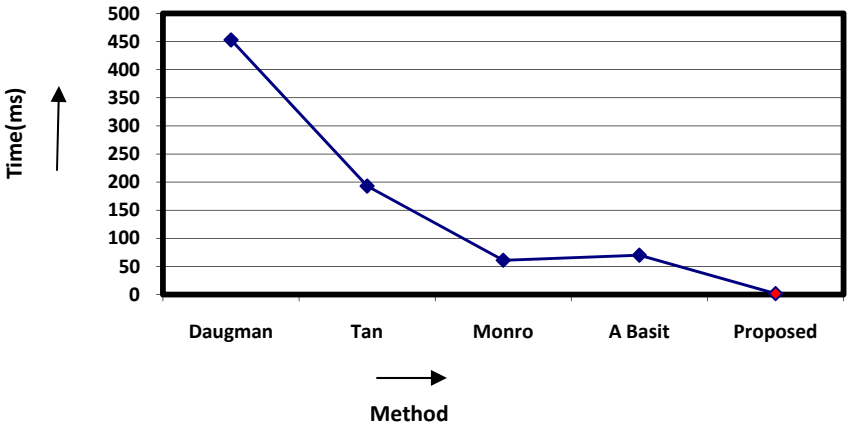

Figure 4.17. Time comparison of feature extraction and matching stage.
(Time in milliseconds)

The graph in Figure 4.18 shows the comparison result of various techniques including the proposed work. The graph is plotted for percentage of correct decisions against the different methods used for various researchers. It can be clearly seen that the proposed technique is outperforming the other techniques. The results are also tabulated in Table 4.10.

Table 4.10. Comparison of correct recognition rate (CRR)

Method	CRR (%)
Daugman	100
Wildes	99.20
Boles and Boashash	92.64
Jaffer	97.3
Ahmad and Araabi (Db2)	95.71
Norate el al (Haar)	97.3
A Basit	94.11
K. Masood	95.9
Proposed	98

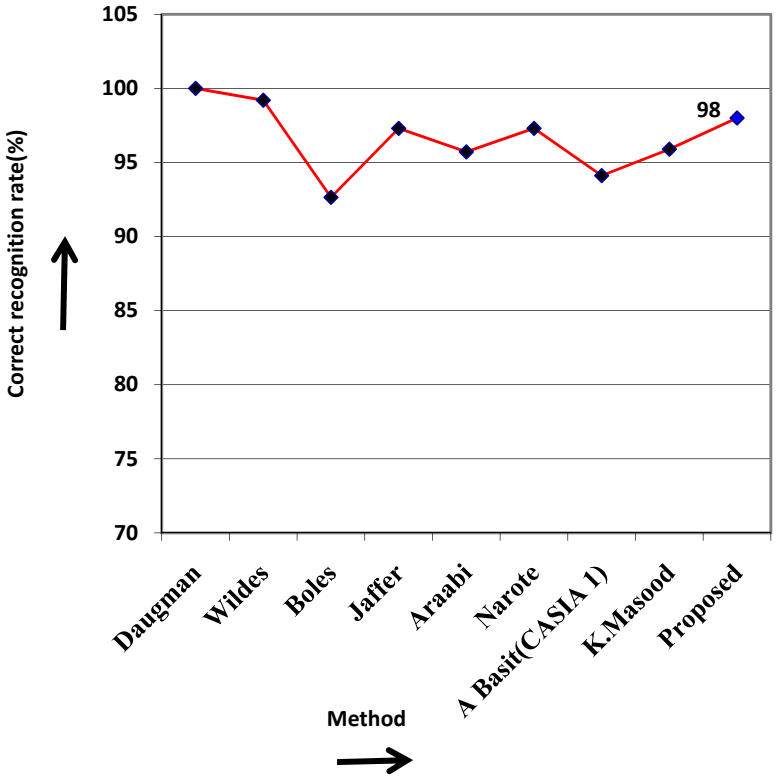

Figure 4.18. Comparison of correct recognition rate (CRR)

CHAPTER 5

CONCLUSIONS AND FUTURE WORK

5.1 Conclusions

Iris recognition system has proved to be the most accurate and efficient method for use in biometrics. The proficiency level achieved by the system provides a user with a high degree of certainty to achieve the desired objectives in security. There is still a lot of potential to improve the speed and achieve 100 percent accuracy in the recognition. The first step is to acquire an image which is processed to localize the iris. Iris effective region is normalized and feature information is extracted to generate a binary feature vector. The feature vectors of enrolled images are stored in database and feature vectors of test images are compared with the templates stored in the database to make a decision that whether it is a match or otherwise.

An endeavor has been made in this research work to propose a robust and swift algorithm for the implementation of the system. The use of basic morphological operations like erosion and dilation with a suitable structuring element has been done with a bit plane slicing technique. The results obtained are quite promising in terms of saving in computational cost of time and achieving the accuracy of 100% in case of the pupil detection when implemented on CASIA version 1. The recognition rate in case of iris outer boundary detection is 99.47%. There are a total of 756 images in the dataset and only 4 x images have not been correctly localized.

The normalization of the iris effective region has been done to get a rectangular image of constant dimensions of size 64 x 180. The normalization process compensates the dimensional variations which occur due to the distance between eye and camera; and due to dilation and contraction of the pupil. Average time taken to normalize the image is 0.0219 seconds.

Feature extraction has been carried out with a simple and straight forward method using bit plane slicing. The method offers reduction in computational cost and matching accuracy of 98%. Comparison with the other techniques shows that the accuracy achieved is optimum. Bit plane 5, 6 and 7 have been used for experiments. Bit plane ‘6’ which shows the contribution of bit ‘5’ in the output image, gives a correct recognition

accuracy of 98%. Moreover, the recognition rate improves as the number of enrolled images increases. The feature extraction is accomplished in just 90 micro seconds giving a saving in time when compared with other techniques using transform domains.

Iris patterns become interesting as an alternative approach to reliable visual recognition of persons when imaging can be done at distances of less than a meter, and especially when there is a need to search very large databases without incurring any false matches despite a huge number of possibilities. In addition, as an internal (yet externally visible) organ of the eye, the iris is well protected from the external harmful effects and remains stable over time. Finally, the ease of localizing eyes in faces, and the distinctive annular shape of the iris, facilitates reliable and precise isolation of this feature and the creation of a size-invariant representation. Research in the iris recognition system has taken strides and it has proved its efficacy by provision of a reliable security.

5.2 Future Work

Since the iris recognition system is an active area of research nowadays, therefore, few recommendations may be considered for the future, for improvement in speed and the accuracy of the algorithm.

- The system may be implemented in the C++ or C# net because MATLAB is slow as it uses the built in functions and consumes lot of memory and time. The flexibility in terms of implementation on different platforms will also be achieved.
- Morphological operators are known due to speed and accuracy. Therefore, use of morphological operators and bit plane slicing may be investigated in other recognition techniques like finger print recognition and blood vessel segmentation.

References

[1] Abdul Basit, "Iris Localization Using Grayscale Texture Analysis and Recognition Using Bit Planes", *PHD Dissertation*, College of Electrical and Mechanical Engineering, National University of Sciences and Technology, Pakistan, Sep 2008.

[2] J. Daugman, "The Importance of Being Random: Statistical Principles of Iris Recognition", *in Pattern Recognition,* vol. 36, No. 2, pp. 279-291, 2003.

[3] Y. Zhu, T. Tan, Y. Wang, "Biometric personal identification based on iris patterns", *Proceedings of the 15th International Conference on Pattern Recognition*, Spain, Vol. 2, 2000.

[4] C. Tisse, L. Martin, L. Torres, M. Robert, "Person identification technique using human iris recognition", *International Conference on Vision Interface*, Canada, 2002.

[5] T. Ruggles, "Comparison of Biometric Techniques", http://www.biometricconsulting.com/bio.htm, 1998.

[6] M. A. Anjum, "Improved Face Recognition using Image Resolution Reduction and Optimization of Feature Vector", *PHD Dissertation*, College of Electrical and Mechanical Engineering, National University of Sciences and Technology, Pakistan, January 2008.

[7] M. Turk and A. Pentland, "Eigenfaces for Recognition", *Journal of Cognitive Neuroscience*, vol. 3, no.1, pp 71-86, 1991.

[8] A. K. Jain, A. Ross and S. Prabhakar, "An Introduction to Biometric Recognition", *IEEE Trans. on Circuits and Systems for Video Technology*, vol. 14, no. 1, pp. 4-20, January 2004.

[9] R. Sanchez-Reillo, C. Sanchez-Avila, and A. Gonzalez-Marcos, "Biometric Identification through Hand Geometry Measurements," *IEEE Trans. on Pattern Analysis & Machine Intelligence*, vol. 22, pp. 1168-1171, 2000.

[10] F. Borowski, "Voice activity detection for speaker verification systems," *Proceedings of SPIE - The International Society for Optical Engineering*, vol. 6937, 2008.

[11] W. M. Campbell, J. P. Campbell, D. A. Reynolds, E. Singer, and P. A. Torres Carrasquillo, "Support vector machines for speaker and language recognition," *Computer Speech and Language*, vol. 20, pp. 210-229, 2006.

[12] R. Plamondon and G. Lorette, "Automatic signature verification and writer identification - the state of the art," *Pattern Recognition*, vol. 22, pp. 107-131, 1989.

[13] R. Plamondon and S. N. Srihari, "On-line and off-line handwriting recognition: A comprehensive survey," *IEEE Transactions on Pattern Analysis and Machine Intelligence*, vol. 22, pp. 63-84, 2000.

[14] P. S. Huang, C. J. Harris, and M. S. Nixon, "Statistical approach for recognizing humans by gait using spatial-temporal templates," *IEEE International Conference on Image Processing*, vol. 3, pp. 178-182, 1998.

[15] C.-Y. Yam, M. S. Nixon, and J. N. Carter, "Gait Recognition by Walking and Running: a Model-Based Approach," in *Asian Conference on Computer Vision (ACCV-2002)*, 2002, pp. 1-6.

[16] A. J. Hoogstrate, H. Van Den Heuvel, and E. Huyben, "Ear identification based on surveillance camera images," *Science and Justice - Journal of the Forensic Science Society*, vol. 41, pp. 167-172, 2001.

[17] B. Moreno, A. Sanchez, and J. F. Velez, "On the Use of Outer Ear Images for Personal Identification in Security Applications," in *IEEE 33rd Annual International Carnahan Conference on Security Technology*, 1999, pp. 469-476.

[18] J. Daugman, "How Iris Recognition Works." *Proceedings of 2002 International Conference on Image Processing*, vol. 1, 2002.

[19] R. Wildes, "Iris Recognition: an Emerging Biometric Technology." *Proceedings of the IEEE,* vol. 85, No. 9, 1997.

[20] N. Ritter. Location of the pupil-iris border in slit-lamp images of the cornea. *Proceedings of the International Conference on Image Analysis and Processing*, 1999.

[21] W. Kong, D. Zhang. Accurate iris segmentation based on novel reflection and eyelash detection model. *Proceedings of 2001 International Symposium on Intelligent Multimedia, Video and Speech Processing*, Hong Kong, 2001.

[22] Y. Zhu, T. Tan and Y. Wang, "Biometric Personal Identification Based on Iris Pattern." *Proceeding of 15th International Conference on Pattern Recognition, Vol. 2, pp. 801-804, 2000.*

[23] L. Ma, T. Tan, Y. Wang, and D. Zhang, "Personal identification based on iris texture analysis," *IEEE Trans. Pattern Analysis and Machine Intelligence*, vol. 25, pp. 1519 1533, 2003.

[24] W. Boles and B. Boashash, "A Human Identification Technique Using Images of the Iris and Wavelet Transform," *IEEE Trans. Signal Processing*, vol. 46, pp. 1185-1188, 1998.

[25] S. Lim, K. Lee, O. Byeon, and T. Kim, "Efficient iris recognition through improvement of feature vector and classifier," *ETRI Journal*, vol. 23, pp. 61-70, 2001.

[26] R. Zhu, J. Yang, and R. Wu, "Iris recognition based on local feature point matching," in *International Symposium on Communications and Information Technologies (ISCIT '06)*. Bangkok, 2006, pp. 451-454.

[27] R. C. Gonzalez and R. E. Woods, "Digital Image Processing", 3rd Edition, Dorling Kindersley Publishing Inc. (India), *2008.*

[28] "Bit Plane," PC Magazine, 2007.

[29] "Bit-plane," http://en.wikipedia.org/wiki/Bit-plane accessed, 2010.

[30] B. L. Bonney, R.W. Ives, D.M. Etter and Y. Du, "Iris Pattern Extraction using Bit Planes and Standard Deviations." *Proceedings of the 38th Asilomar Conference on Signals, Systems and Computers, Pacific Grove, CA, pp. 582-586, November 2004.*

[31] Chinese Academy of Sciences-Institute of Automation (CASIA), Iris Image Database, *http://www.sinobiometrics.com*.

[32] E. Wolff. *Anatomy of the Eye and Orbit*. 7th edition. H. K. Lewis & Co. LTD, 1976.